

Benchmark of numerical modeling approaches on the systematic performance evaluation of wave energy converters

Tan, Jian; Coe, Ryan G.; Lavidas, George

DOI

10.1016/j.apor.2025.104725

Publication date

Document Version Final published version

Published in Applied Ocean Research

Citation (APA)
Tan, J., Coe, R. G., & Lavidas, G. (2025). Benchmark of numerical modeling approaches on the systematic performance evaluation of wave energy converters. *Applied Ocean Research*, *162*, Article 104725. https://doi.org/10.1016/j.apor.2025.104725

Important note

To cite this publication, please use the final published version (if applicable). Please check the document version above.

Copyright

Other than for strictly personal use, it is not permitted to download, forward or distribute the text or part of it, without the consent of the author(s) and/or copyright holder(s), unless the work is under an open content license such as Creative Commons.

Please contact us and provide details if you believe this document breaches copyrights. We will remove access to the work immediately and investigate your claim.

ELSEVIER

Contents lists available at ScienceDirect

Applied Ocean Research

journal homepage: www.elsevier.com/locate/apor



Research paper

Benchmark of numerical modeling approaches on the systematic performance evaluation of wave energy converters

Jian Tan alo,*, Ryan G. Coe blo, George Lavidas alo

- ^a Faculty of Civil Engineering and Geosciences, Delft University of Technology, Stevinweg 1, 2628 CN, Delft, The Netherlands
- ^b Sandia National Laboratories, Albuquerque, NM, USA

ARTICLE INFO

Keywords: Numerical modeling Wave energy converter Power Fatigue Levelized cost of energy

ABSTRACT

Different numerical modeling methods have been developed and applied to evaluate a variety of performance indicators of wave energy converters (WECs), including the power performance, structural loads, levelized cost of energy, etc. Based on the modeling fidelity, the commonly used numerical modeling approaches can be classified as linear modeling, weakly nonlinear modeling and fully nonlinear modeling approaches. Each method differs in accuracy and computational efficiency, making them suitable for different stages of WEC design. However, the selection of modeling approach could significantly impact evaluation outcomes. For instance, simplified linear models may underestimate structural loads or overestimate energy production in some operational conditions, potentially leading to less cost-effective designs. Given the widespread utilization of these models, it is essential to understand the uncertainties brought by them in performance evaluations.

This work is dedicated to benchmarking different linear-potential-flow-based numerical models for evaluating the systematic performance of WECs. Three representative numerical modeling approaches are considered in this work, including linear frequency-domain modeling, statistically linearized spectral-domain modeling and Cummins equation-based nonlinear time-domain modeling. A generic point absorber WEC is considered as the research reference in this work, and different sea sites are taken into account. The numerical models are utilized to predict critical performance indicators, including power performance, the annual energy production, the capacity factor, the levelized cost of energy and the PTO fatigue loads. By comparing the results, this work identifies the uncertainties associated with different modeling approaches in evaluating WEC performance.

1. Introduction

Ocean wave energy represents a vast, sustainable resource with high energy density, offering imperative potential for the global energy transition (Lavidas and Venugopal, 2017; Jin and Greaves, 2021). However, the commercialization scale of wave energy conversion technologies is far behind other offshore renewable energy technologies, such as offshore wind and offshore solar power. This is primarily due to its higher levelized cost of energy compared to other technologies (Martinez and Iglesias, 2022). Hence, to fully unlock the potential of ocean wave energy, it is significant to advance the design iteration towards more efficient and reliable wave energy converters (WECs) (Guo and Ringwood, 2021).

Numerical modeling has become a crucial tool for the early-stage design and optimization of WECs, as it significantly reduces both costs and time compared to physical experiments (Guo and Ringwood, 2021). These models offer valuable insights into WEC dynamics, loads, and power performance, enabling the evaluation of WECs across various

performance aspects. Commonly used modeling approaches in WECs include potential flow theory-based models and fully nonlinear Computational Fluid Dynamics (CFD) models (Folley, 2016). These approaches vary in computational efficiency and modeling fidelity, making them suitable for different design stages and purposes.

CFD models are developed to numerically solve the Navier–Stokes equations, and their solution methods can be further classified into mesh-based and mesh-less solvers (Davidson and Costello, 2020). Mesh-based CFD software, such as OpenFOAM, Fluent, and STAR-CCM+, solves the incompressible Navier–Stokes equations by discretizing the computational domain into nodes and cells. In mesh-based solvers, the Volume-of-Fluid method is commonly employed for free-surface phenomena to facilitate the modeling of wave breaking, slamming, and overtopping (Li and Yu, 2012a; Coe and Neary, 2014). Mesh-less methods, also known as Smoothed Particle Hydrodynamics (SPH), discretizes the domain into Lagrangian particles to solve the Navier–Stokes equations (Crespo et al., 2015). It is particularly suitable for

^{*} Corresponding author.

E-mail address: J.tan-2@tudelft.nl (J. Tan).

modeling strong nonlinear free-surface effects (Gomez-Gesteira et al., 2010). DualSPHysics is an open-source SPH code which has recently received much research interest in WEC modeling (González-Cao et al., 2024). Nevertheless, owing to their high computational demands, CFD models are predominantly adopted for survivability assessments of WECs, rather than for estimating long-term statistical metrics such as average power output and accumulated fatigue damage (Ransley et al., 2017).

Potential flow theory has a prolonged history serving as a foundation for modeling WECs (Falnes, 2003). Different from Navier-Stokes equations-based methods, potential flow theory is based on the assumptions of inviscid, incompressible, and irrotational flow (Folley et al., 2019). These assumptions enable the simplification of the governing equations to Laplace's equation for the velocity potential (Papillon et al., 2020). Different models have been developed to solve the linear potential problems, ranging from the fully linearized approach to the fully nonlinear approach. In the linearized potential flow modeling, small wave amplitudes and body motions are assumed to allow for the linearization of boundary conditions and wave-body interactions. Typically, these models are solved in the frequency domain through the application of the Boundary Element Method (BEM), vielding hydrodynamic parameters including excitation forces and radiation coefficients. WAMIT, AQWA and Nemoh are the commonly used tools for solving linear potential problems of floating bodies (Sheng et al., 2022). As an extension, weakly nonlinear potential flow-based models can be applied to address some limitations of the fully linearized potential flow models. Weakly nonlinear potential flow method retains the assumptions of the mean free surface and mean wetted surface while enhancing the solution accuracy via a perturbation scheme (Davidson and Costello, 2020). In the perturbation scheme, the Taylor series expansion of the free surface and body boundary conditions about their mean positions is included. In addition, some studies have proposed partial nonlinear potential flow methods for WECs by considering the time-dependent body boundary conditions on the instantaneous wetted surface. This type of method could extend the linear-potential flowbased models to cover some selected nonlinear effects (Merigaud et al., 2012). Representing the high fidelity of the potential flow theory, fully nonlinear potential flow modeling lifts the small-amplitude assumption by solving Laplace's equation with the intact free-surface boundary condition and the fluid domain of instantaneous nonlinear wettedsurface (Folley, 2016). The prevalent solution methods for the fully nonlinear potential flow modeling include the higher-order boundary element methods (Teng and Taylor, 1995), mixed Eulerian-Lagrangian methods (Kashiwagi, 2000) and spectral methods (Fenton and Rienecker, 1982). This modeling approach can be applied to derive the wave-body interaction problems with much higher fidelity.

Among the modeling methods mentioned, linear potential flowbased models are the most commonly used for identifying systematic performance indicators of WECs during the early to middle stages of design, due to their superior computational efficiency (Pecher, 2017). Accordingly, this work primarily focuses on numerical modeling approaches based on linear potential flow theory. This type of modeling approaches can be further classified as Frequency-Domain (FD) models, Spectral-Domain (SD) models, and Cummins equation-based Time-Domain (TD) models (Folley, 2016). As reviewed in Penalba Retes et al. (2015), frequency-dependent hydrodynamic coefficients can be efficiently derived by applying linearized boundary conditions in an idealized fluid. These coefficients are crucial for formulating the equation of motion of floating structures in the frequency domain. Although linear FD modeling is computationally efficient and requires minimal time, it is limited to fully linear analyses (Li and Yu, 2012a), which restricts its accuracy for simulating WECs operating in high-wave environments or at large motion amplitudes. Comparatively, Cummins equation-based TD modeling is also derived based on linear potential flow theory (Cummins et al., 1962). However, it numerically solves the dynamics of the floating structure at each time step, enabling

the incorporation of selected nonlinear effects as correction terms. Although TD models offer greater accuracy than FD and SD models, particularly for high-wave conditions, they require significantly more computational time than FD and SD models due to the need for numerical integration (Tan et al., 2022b; Ricci et al., 2008). Nevertheless, Cummins equation-based TD models are still considered much more computationally efficient but less accurate than CFD models under circumstances with highly pronounced nonlinear effects, such as survivability analyses (Li and Yu, 2012a). SD models, as an alternative, extend the FD modeling by incorporating nonlinearities via statistical linearization (Folley, 2016), thereby providing a balanced compromise between computational efficiency and simulation accuracy. SD models have been extended to capture a variety of nonlinear effects, including quadratic damping (Silva et al., 2020), excitation force decoupling in oscillating surge WECs (Folley and Whittaker, 2010), PTO force capping (Tan et al., 2022b), and end-stop mechanisms (Silva, 2019; Da Silva et al., 2020). More recently, SD modeling has been extended to cover the full wave-to-wire process of WECs, integrating both hydrodynamic and electrical system responses (Tan et al., 2023; Tan and Laguna, 2023).

A variety of performance indicators for WECs have been evaluated through numerical models, including power performance, loads, annual energy production (AEP), and the levelized cost of energy (LCOE). Among these, power performance is predominantly emphasized during early-stage design, as power generation is the primary function of WECs. In Pastor and Liu (2014), both TD and FD models were used to calculate the power production of a heaving point absorber WEC. A guideline for applying FD modeling to estimate the energy production of WECs was proposed in Bosma et al. (2012), where a two-body point absorber WEC was used as a generic reference. In Cheng et al. (2014), an FD model was employed to predict the power capture width of a point absorber WEC, considering the effects of buoy size and PTO damping. In Babarit et al. (2012), TD modeling was used to model eight different types of WECs, providing detailed power performance and annual energy production data for WECs at three European sea sites. The power performance of a novel dense-located WEC array was estimated using FD modeling in Wei et al. (2017). In Taghipour and Moan (2008), an FD model was developed to assess the power performance of a multi-body WEC. Similarly, in Tan et al. (2021), FD modeling was applied to predict the power production of a heaving WEC with varying buoy sizes and PTO control strategies. Additionally, Amini et al. (2021), Jin et al. (2023) estimated the power production of different types of WECs at realistic sea sites using the open-source TD modeling tool WEC-Sim (Lawson et al., 2014). Furthermore, SD modeling has also been employed to calculate the power performance and annual energy production of WECs, incorporating nonlinear effects (Tan et al., 2022a,b).

The techno-economic metrics, such as the LCOE, could provide valuable insights into the cost-effectiveness of WECs. The evaluation of the techno-economic performance for WECs has garnered significant research interest in recent years. In Zhong et al. (2024), the AEP and the LCOE of a newly proposed mass-adjustable-buoy-based WEC were estimated through a combination of TD modeling and economic modeling. In Tan et al. (2022c, 2020), FD modeling was applied to analyze the effects of buoy and PTO sizing on the AEP and the LCOE of a heaving point absorber WEC. A techno-economic study in Petracca et al. (2022) assessed the LCOE of WECs connected to a floating wind platform, using TD modeling via the WEC-Sim tool, with a focus on a sea site off the coast of Northern Ireland. A novel bean-float type WEC was modeled in Chandrasekaran and Sricharan (2021) using TD modeling, and the LCOE was further analyzed for various Indian sea states. The AEP and the LCOE of an oscillating water column (OWC) type WEC were estimated in Rosati and Ringwood (2023) based on TD modeling, with consideration given to the influence of PTO control strategies. The study concluded that LCOE is more sensitive to PTO size than to the bypass valve size of the turbine. Additionally, recent technoeconomic studies have utilized SD modeling to assess the performance of WECs. For example, Bonfanti and Giorgi (2022), Tan et al. (2022b) studied the techno-economic performance of different WEC types using the SD modeling approach.

Identifying the loads exerted on WECs is crucial for designing systems that can reliably withstand highly variable and harsh wave climates. Offshore structures are typically subjected to two types of loading: extreme loading and fatigue loading. While extreme loading is important, the focus here is on fatigue loading. Fatigue loading primarily occurs during regular operation, resulting from cyclic stress variations over time that accumulate strain and wear on the structure. It is worth noting that there are various methods for fatigue damage analysis, including the FD method (e.g., Dirlik method) and the TD method (e.g., Rainflow counting method) (Muñiz-Calvente et al., 2022). However, the FD, SD, and TD modeling methods discussed in this work mainly refer to different approaches for simulating the dynamics of WECs subjected to wave excitations. The predicted dynamics are needed subsequently to serve as input for fatigue analysis. Several studies have utilized numerical modeling to investigate the fatigue loading on WECs (Zurkinden et al., 2015; Shahroozi et al., 2022; Ballard et al., 2020). In Zurkinden et al. (2013), FD WEC dynamic modeling was used to calculate the dynamics of a point absorber WEC and the loads on the connection area between the PTO system and the WEC arm across variable sea states. The accumulated fatigue damage was derived assuming a narrow-band process. Similarly, in Liu et al. (2019), FD modeling was employed to estimate the fatigue load on the hydraulic PTO system of a WEC, considering a realistic sea site to assess the fatigue reliability of the WEC. The TD WEC dynamic modeling approach has also been widely applied in studies that explore the fatigue loads on WECs. For instance, in Shahroozi et al. (2022), a TD WEC dynamic model was used to quantify fatigue loads on the mooring lines and PTO connection area of a point absorber WEC. In Nielsen et al. (2017), TD modeling was used to optimize the PTO control strategy for a point absorber WEC, considering both power losses and fatigue damage. In comparison, to the best of the authors' knowledge, the SD modeling approach has not yet been applied to support the identification of fatigue loads on WECs. This is primarily because the SD modeling approach is still relatively new compared to FD and TD models.

As discussed above, the FD, SD, and TD modeling methods have been used to evaluate various aspects of WEC performance, significantly contributing to the development of wave energy conversion technology. However, these models differ in terms of modeling fidelity, which can lead to deviations in the evaluation results. Besides, different performance indicators of WECs may present different sensitivities to numerical modeling fidelity. For instance, the linear FD model could overestimate the power performance under powerful sea states, while this overestimation may have a negligible impact on the AEP if the considered wave resource is generally mild. Comparatively, the overestimation of structural loads at powerful sea states, even with rare occurrence probability, could result in a noticeable deviation in the prediction of total accumulated fatigue damage. This is because the number of cycles to failure in the S-N curve is exponential to load amplitude (Jimenez-Martinez, 2020). Similarly, techno-economic metrics may also exhibit different levels of sensitivity to numerical modeling approaches. To the best of the author's knowledge, there is currently no study that quantitatively investigates the influence of modeling approaches on the overall performance assessment of WEC systems. Therefore, it is essential to establish a benchmark for these modeling approaches, focusing on some key elements in systematic performance evaluation with considering various wave climates. In this study, a generic heaving point absorber with a nonlinear PTO system is considered. The three WEC dynamic models, namely the FD, SD, and TD models, are applied to estimate the WEC's performance in three aspects: power production, the techno-economic metrics, and

fatigue damage. The critical area for fatigue loading is defined as the connection rods between the PTO system and the floating buoy. Longterm wave data from several realistic sea sites are incorporated, and a preliminary economic model is applied to analyze the techno-economic metric, LCOE. For fatigue prediction, the Dirlik method is applied to the stress loads calculated by each WEC dynamic model to derive fatigue damage across various sea states. The performance indicators evaluated by the three models are presented and compared, highlighting the discrepancies between the FD and SD models relative to the nonlinear TD model.

2. Methodology

2.1. WEC description

A cylindrical heaving point absorber is considered in this study to represent a generic WEC concept, as illustrated in Fig. 1. The WEC floater is connected via rigid rods to the PTO system, which is bottom-founded at the sea floor. Three identical rigid rods are placed parallel to distribute the vertical compressive and tensile loads. As the PTO rods are expected to endure numerous cyclic loads during the service life, the fatigue analysis of this work is focused on the stress loading exerted on the cross-sectional plane of the PTO rod. A passive PTO system is utilized in this WEC system, and the PTO force saturation mechanism is incorporated to protect the electrical component from being overheated (Prado and Polinder, 2013). An end-stop force mechanism is implemented at both ends of the PTO system to avoid the huge impact force. Assuming the wave period of 8 s to be a rated operation condition, the nominal power rating of the WEC system is then roughly defined as

$$P_{rated} \approx \frac{2\pi}{8} Z_{es} F_m$$
 (1)

where P_{rated} is the nominal rated power; Z_{es} and F_m denote the end-stop displacement limit and the PTO force limit. The relevant parameters of the WEC concept are specified in Table 1. Specifically, the drag coefficient C_d is set to 1, following the Palm and Eskilsson (2021), in which the same floater shape as that used in this work was utilized. The end-stop displacement limit Z_{es} is selected based on the physical constraints of the PTO system. Assuming a linear generator as the PTO. as reported in Tan et al. (2022c), the optimized translator length for a linear permanent magnet generator is approximately 3 m, with the force limit F_m of 200 kN. Accordingly, Z_{es} is defined as 1.6 m, slightly exceeding half the translator length. Larger displacements would result in an overlap of less than 50% between the stator and translator, leading to reduced generator conversion efficiency. The end-stop spring stiffness K_{es} is chosen to match the relatively soft spring used in Chen et al. (2021), which concluded that a relatively soft spring enhances power absorption. Although it is known that both Z_{es} and K_{es} significantly influence the dynamics and power performance of WECs, further discussion is clearly beyond the scope of this study. These aspects have been comprehensively addressed in Chen et al. (2021), Palm and Eskilsson (2021).

2.2. Numerical modeling of WEC dynamics

2.2.1. Linear frequency-domain modeling

Assuming a fully linear system, the equation of motion of the WEC can be formulated in the frequency domain. The dynamics of the WEC can be described in the form of complex amplitudes under each frequency component (Falnes, 2003), as

$$\hat{F}_{e}(\omega) = \hat{z}(\omega) \left\{ -\omega^{2} \left[m + M_{r}(\omega) \right] + K_{hs} + i\omega \left[R_{r}(\omega) + R_{pto} \right] \right\}$$
 (2)

where ω is the angular frequency of the incoming wave, and $\hat{}$ is the symbol of the complex amplitude; \hat{z} is the complex amplitude of the displacement; \hat{F}_e embodies the complex amplitude of excitation force,

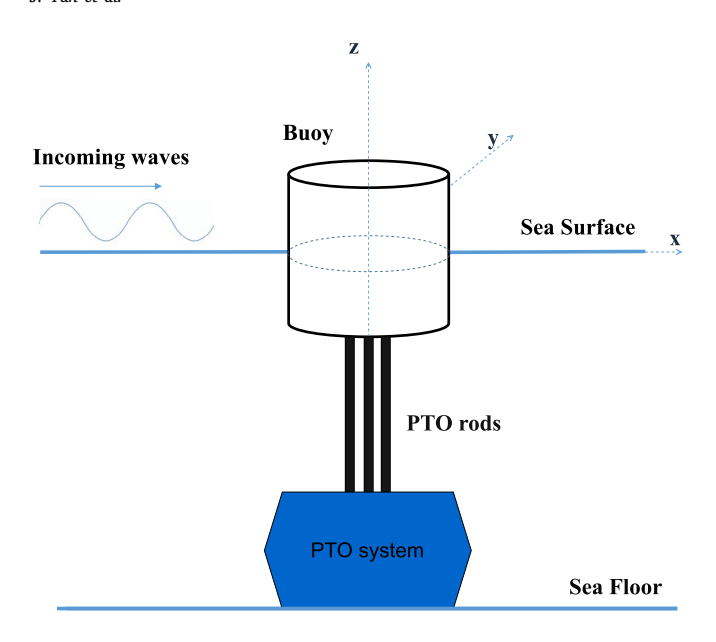


Fig. 1. Schematic of the cylindrical heaving point absorber WEC with a bottom-founded PTO system.

Table 1
Relevant parameters of WEC system

Parameters	Quantities
Cylinder radius	5 m
Cylinder height	10 m
Cylinder mass: m	402520 kg
Water-plane area: A_s	78.5 m ²
Buoy draft	5 m
PTO force limit: F_m	200 kN
End-stop displacement limit: Z_{es}	1.6 m
End-stop spring stiffness: K_{es}	500 kN/m
Nominal power rating: P_{rated}	250 kW
PTO rod cross-sectional area	$3 \times 23 \text{ cm}^2$
Water depth	50 m
Drag coefficient: C_d	1
Water density: ρ	1025 kg/m^3

 K_{hs} stands for the hydrostatic coefficient; $M_r(\omega)$ and $R_r(\omega)$ are the frequency-dependent added mass and radiation damping coefficients; m represent the mass of the floater. The hydrodynamic coefficients throughout this work, including M_r , K_{rad} and F_e , are calculated by a linear BEM solver, namely Nemoh (Penalba et al., 2017a).

Limited to the linear assumption in the FD modeling, the viscous drag effect and the end-stop mechanism are neglected. The PTO force in the FD model is given in a linear form by neglecting the saturation effect, as

$$\hat{F}_{pto,lin}(\omega) = -i\omega \hat{z}(\omega) R_{pto} \tag{3}$$

The mean power absorption in the FD modeling can be calculated as

$$\overline{P}_{ab,FD} = \sum_{i=1}^{N} \frac{1}{2} R_{pto} \left| i\omega \hat{z}(\omega) \right|^2 = R_{pto} \sigma_{\dot{z}}^2$$
(4)

where $\sigma_{\dot{\tau}}$ denotes the standard deviation of the velocity of the WEC.

2.2.2. Nonlinear time-domain modeling

As the device in this paper is assumed to oscillate in heave motion, the numerical model is only discussed for this degree of freedom. According to Cummins equation (Cummins et al., 1962), the equation of motion of a floating rigid buoy can be described in the time domain as

$$[m + M_r(\infty)]\ddot{z}(t) = F_e(t) + F_{pto,sq}(t) + F_{es}(t) + F_{vis}(t) + F_{hs}(t)$$

$$+ \int_{-\tau}^{\tau} K_{rad}(t-\tau)\dot{z}(\tau)d\tau \tag{5}$$

where M and $M_r(\infty)$ are the body mass and the added mass evaluated at the infinite frequency, and K_{rad} is the radiation impulse function; z, \dot{z} and \ddot{z} stand for the displacement, the velocity and the acceleration of the rigid body; F_e , $F_{plo,sa}$, F_{es} , F_{vis} and F_{hs} denote the wave excitation force, PTO force, end-stop force, viscous drag force and the hydrostatic restoring force respectively. The convolution term on the right-hand side of the equation describes the memory effect of the radiation force.

The hydrostatic force of the WEC is calculated as:

$$F_{hs} = -K_{hs}z(t) \tag{6}$$

Considering the saturation effect, the PTO force can be described as

$$F_{pto,sa}(t) = \begin{cases} -R_{pto}\dot{z}(t), & for \quad |R_{pto}\dot{z}(t)| \le F_m \\ \operatorname{sign}[-R_{pto}\dot{z}(t)]F_m, & for \quad |R_{pto}\dot{z}(t)| > F_m \end{cases}$$
(7)

where R_{pto} is the PTO damping coefficient, and F_m is the PTO force limit, defined as 200 kN.

The end-stop mechanism takes effect once the moving component exceeds a defined limit, preventing the hard collision. It can be modeled as springs located at the two ends of the PTO system, and the end-stop force is then given as

$$F_{es}(z) = \begin{cases} -K_{es}(z + Z_{es}), & for \quad z \le -Z_{es} \\ \\ 0, & for \quad |z| < Z_{es} \\ \\ -K_{es}(z - Z_{es}), & for \quad z \ge Z_{es} \end{cases}$$
 (8)

where K_{es} and Z_{es} represent the end-stop spring stiffness and the stroke limit where the end-stop mechanism begins to take effect. In this study, K_{es} is set to be 500 kN/m and Z_{es} is set to be 1.6 m.

The viscous drag effect can be incorporated as a quadratic damping term (Journée et al., 2015; Silva et al., 2020), expressed as

$$F_{vis} = -\frac{1}{2}\rho C_D A_D |\dot{z}(t)| \dot{z}(t) \tag{9}$$

where C_d embodies the drag coefficient which is defined as 1 in this study, and A_s denotes the projected area of the cylindrical buoy.

With the time-dependent responses derived, the mean absorbed power estimated by the TD modeling is calculated

$$\overline{P}_{ab,TD} = \frac{1}{T} \int_{t-0}^{T} -F_{pto,sa}(t)\dot{z}(t)dt$$
 (10)

where T corresponds to the simulation time duration.

The nonlinear TD model described above is implemented using the open-source software WEC-Sim (Lawson et al., 2014). As a widely recognized tool in the field of WECs, WEC-Sim has been validated and applied in a range of relevant studies (Ruehl et al., 2014, 2016; Jin et al., 2023; Ogden et al., 2022). Therefore, the WEC-Sim model used in this study is considered as the numerical experiment that provides more accurate results than the linear FD model and the SD model applied in this work. In WEC-Sim, the convolution integral in (5) is approximated using a state-space representation derived from the computed hydrodynamic coefficients, with the goal of reducing computational cost. The same set of hydrodynamic coefficients used in the linear FD model is applied in the WEC-Sim implementation in this work. The identification of the state-space parameters is realized in the time domain using the singular value decomposition method, as detailed in Tom et al. (2015). The time-dependent responses of the system are solved using a numerical integration scheme and realized through a Simulink model (Lawson et al., 2014). The ODE 45 Solver in Matlab is selected as the solution algorithm. The Simulink model constructed for this work is shown in Fig. 2. To evaluate the WEC's performance under more realistic conditions, irregular sea states are considered in all simulation cases, and the JONSWAP spectrum is applied (Journée

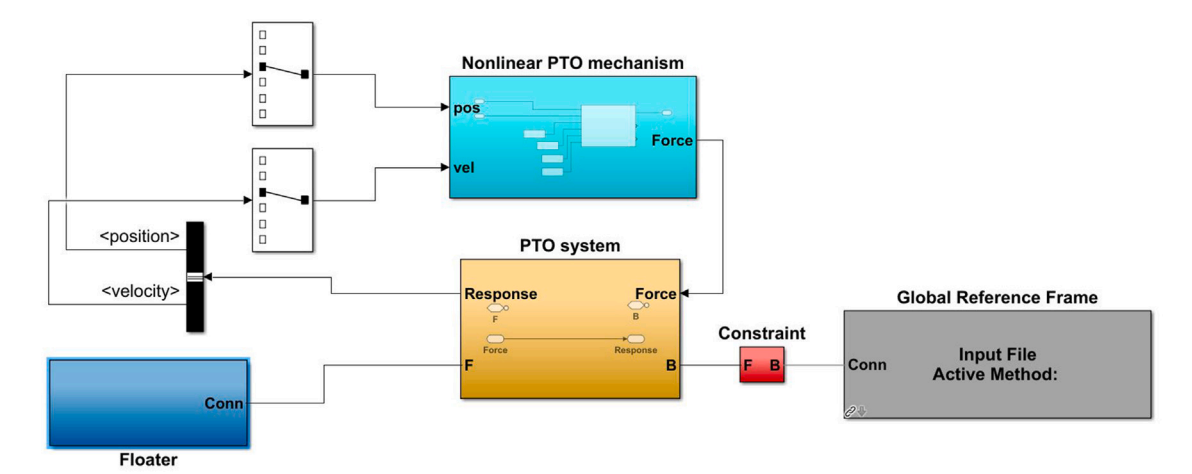


Fig. 2. Simulink model of the WEC system utilized in WEC-sim.

et al., 2015). Additionally, the time duration of each simulation is set to 3600 s and the period of initial 100 s is implemented as a ramp time to avoid strong transient flow (Ruehl et al., 2014). The derived WEC response data during the ramp time is excluded in the post-processing phase. The time step in all the TD simulations is defined as 0.05 s. In order to make a statistically robust measure from time-dependent nonlinear results, each simulation is repeated ten times to obtain the averaged values of the absorbed power and the power spectral density (PSD) of the WEC responses at each frequency. The PSD values are derived using the Fast Fourier Transform (FFT) for time-dependent data calculated by TD modeling. It should be noted that the simulation time duration in TD models could make a difference to the results (Kvittem and Moan, 2015; Gao et al., 2023). However, as suggested in Kvittem and Moan (2015), a 1-hour simulation duration is mostly sufficient to capture the important fatigue effects in floating wind structures which is comparable to the system studied in this work. Therefore, using a 1-hour duration is considered reasonable, particularly considering the heavy computational demands of TD simulations.

2.2.3. Spectral-domain modeling

SD modeling is built upon the structure of FD modeling, while nonlinear effects can be incorporated by statistical linearization. The equation of motion of the WEC in the SD modeling can be given as

$$\begin{split} \hat{F}_{e}(\omega) &= \hat{z}(\omega) \left\{ -\omega^{2} \left[m + M_{r}(\omega) \right] + K_{es,eq}(\omega) + K_{hs} \right. \\ &+ \mathrm{i}\omega \left[R_{r}(\omega) + R_{vis,eq} + R_{pto,eq} \right] \right\} \end{split} \tag{11}$$

where $K_{es,eq}$, $R_{vis,eq}$ and $R_{pto,eq}$ denote the equivalent end-stop stiffness, the equivalent viscous drag damping, and the equivalent PTO damping. They are obtained via the statistical linearization and included in the equation of motion to represent the contribution of the corresponding nonlinear effects to the dynamics of the WEC.

The mathematical derivation of statistical linearization is detailed in Appendix A. Referring to (A.4), the equivalent linearized coefficients concerned in this study can be derived as

$$K_{es,eq} = \frac{\langle zF_{es}(z)\rangle}{\langle z^2\rangle} \tag{12}$$

$$R_{vis,eq} = \frac{\langle \dot{z}F_{vis}(\dot{z})\rangle}{\langle \dot{z}^2\rangle} \tag{13}$$

$$R_{pto,eq} = \frac{\langle \dot{z} F_{pto,sa}(\dot{z}) \rangle}{\langle \dot{z}^2 \rangle} \tag{14}$$

Taking the equivalent coefficient of the end-stop force, $K_{es,eq}$, as an example, the other two can be derived similarly. Assuming the responses of the WEC system strictly follow a Gaussian process, then the

probability density function of the responses can be given as

$$K_{es,eq} = \int_{-\infty}^{\infty} \frac{z F_{es}(z)}{\sigma_z^2} p(z) dz$$
 (15)

where p(z) embodies the probability density function of the WEC response z, which can be given as

$$p(z) = \frac{1}{\sigma_z \sqrt{2\pi}} \exp(-\frac{z^2}{2\sigma_z^2})$$
 (16)

 $K_{es,eq}$ can therefore be solved by substituting (16) into (15).

It can be noticed that the linearized coefficients in SD modeling depend on the standard deviation of the responses, which is unknown prior to solving the system. To address this, an iterative scheme is employed, starting with an initial guess based on the FD model results (Tan et al., 2022b; Folley and Whittaker, 2010). The process proceeds until the specified tolerance is met, and the tolerance in this work is defined as 1×10^{-5} across all the simulation cases. The workflow of the SD modeling can be visually summarized in Fig. 3.

The WEC responses can be determined by solving (11). Subsequently, the complex amplitude of the PTO force can be described as

$$F_{pto,eq}(\omega) = -i\omega \hat{z}(\omega) R_{pto,eq}$$
 (17)

The mean power absorption is given as

$$\overline{P}_{ab,SD} = \sum_{i=1}^{N} \frac{1}{2} R_{pto,eq} |i\omega \hat{z}(\omega)|^2 = R_{pto,eq} \sigma_{\hat{z}}^2$$
(18)

2.3. PTO damping tuning

The selection of the PTO damping plays a significant role in the power absorption. As demonstrated in Hals et al. (2002), the optimal PTO damping for an ideally linear WEC system without any mechanical losses is given as

$$R_{pto}(\omega) = \sqrt{R_r(\omega)^2 + X(\omega)^2}$$
 (19)

where $R_{pto}(\omega)$ is the tuned PTO damping for a WEC at the specified wave frequency ω . The intrinsic reactance X is expressed as

$$X(\omega) = \omega [M_r(\omega) + m(\omega)] - \frac{K_{hs}}{\omega}$$
 (20)

It is visible that the optimal PTO damping, R_{pto} , depends on the wave frequency, indicating that this method was initially applicable to regular wave conditions. To adapt it for irregular sea states, the energy period, T_e , is employed as an equivalent to the wave period in regular wave scenarios, referring to Tan et al. (2021). It should be noted that this is only a simplified method to tune the PTO damping for WECs

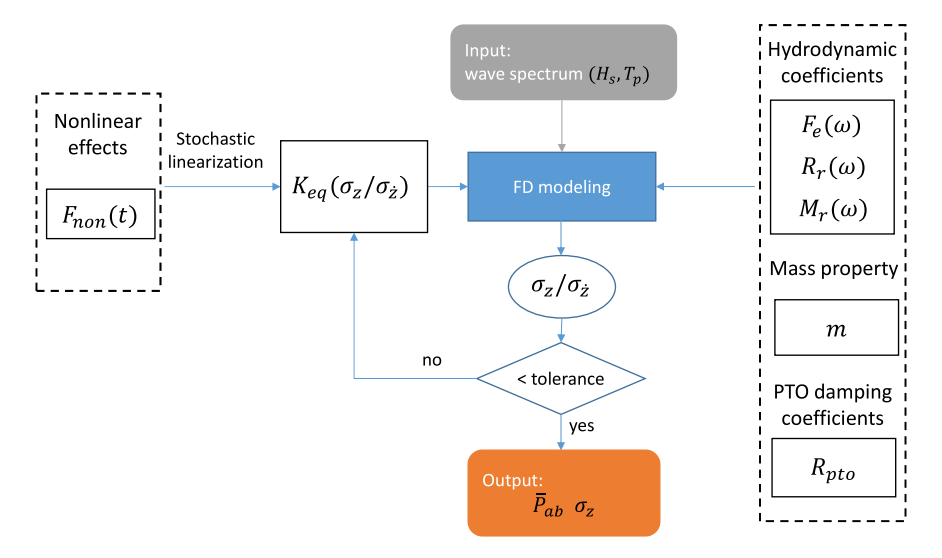


Fig. 3. Workflow of implementing SD modeling for WECs.

 Table 2

 Information of considered environmental inputs.

Sea site	Data type	Country
California	NDBC buoy data	USA
North Sea	spectral-wave model data	Netherlands
Yeu island	Candhis buoy data	France

subjected to irregular waves. At the same time, it is not necessarily associated with maximum power output. First, tuning the PTO parameters to the energy period could not guarantee the optimal PTO damping in irregular wave conditions. Secondly, the PTO tuning method does not account for nonlinear effects. Nonetheless, all three WEC dynamic models employ the same set of PTO damping coefficients, a choice deemed reasonable given the benchmarking objective of this study.

2.4. Environmental inputs

Three sea sites are considered in this study as wave climate inputs for the performance evaluation, as shown in Table 2. The scatter diagrams depicting the occurrence of hours of each sea state at these locations are shown in Figs. 4(a), 4(b), and 4(c). Fig. 4(a) represents the wave resource at a site off the coast of California, USA. The wave data for this site is derived from spectral measurements recorded by NDBC Buoy 46022, covering the period from 1996 to 2024 (van Rij et al., 2019). Fig. 4(b) corresponds to a site in the Wadden Sea, Netherlands, part of the North Sea. The wave data for this location is sourced from the ECHOWAVE database, which is generated using a high-resolution spectral wave model (Alday Gonzalez and Lavidas, 2024). This dataset spans from 1992 to 2021, with a temporal resolution of 30 min. Fig. 4(c) presents the scatter diagram for Yeu Island, located in the oceanic territory of France. The wave resource data for this site has been provided in Babarit et al. (2012).

2.5. Economic modeling

To estimate the LCOE of the WEC, a preliminary economic model is applied in this work, referring to Tan et al. (2021). The first step is to calculate the Capital cost (CAPEX) of the WEC system, and the CAPEX can be divided into two parts:

$$CAPEX = C_{Mass} + C_{Power} (21)$$

where C_{Mass} and C_{Power} embody the mass-related costs and the power-related costs. These components can be further defined as:

$$C_{Mass} = C_S + C_{FM} + C_I = \left(\frac{P_{FM}}{P_S} + \frac{P_I}{P_S} + 1\right)C_S$$
 (22)

$$C_{Power} = C_P + C_C = \left(\frac{P_C}{P_P} + 1\right) C_{PTO}$$
(23)

where C_S , C_{FM} , and C_I represent the costs of the structure, foundation & mooring, and installation, respectively, while C_P and C_C correspond to PTO and grid connection costs. The associated cost percentages of CAPEX are 38.2%, 19.1%, 10.2%, 24.2%, and 8.3% (Tan et al., 2021). It is noted that the identified techno-economic metrics would vary with the economic parameters. However, these parameters are defined to be identical when analyzing all the WEC models' results, which could contribute to a reasonable comparison for WEC models.

Referring to the reports (IMARC Group, 2024; Shipbuilding Steel, 2024), the marine stainless steel price, as of Q3 in 2024, was 3670 US dollars per metric tonne in the European market, and the hot-rolled band steel was around 750 US dollars per metric tonne. Given the fact that offshore structure manufacturing requires the combined use of multiple types of steel. The average steel price of the WEC structure is roughly estimated to be 1 Euro/kg, considering the currency exchange rate of 1.06. The buoy density is taken as half that of water. The PTO system is modeled as a direct drive generator, with costs based solely on the generator. The required active material depends on the PTO force limit and generator force density. As in Polinder (2013), a force density of 44 kN/m² is assumed, within the typical 30–60 kN/m² range. The estimated cost of active material in series production is 14,600 Euros/m² (Tan et al., 2021), with total PTO costs set at twice this value to account for manufacturing.

The annual OPEX is assumed to be 8% of CAPEX, while the discount rate r is 8% over a 20-year lifespan, as per (De Andres et al., 2016). The LCOE is then calculated as:

$$LCOE = \frac{CAPEX + \sum_{t=1}^{n} \frac{OPEX_{t}}{(1+r)^{t}}}{\sum_{t=1}^{n} \frac{AEP_{t}}{(1+r)^{t}}}$$
(24)

where n is the lifespan in years, and t represents the evaluated year. The AEP at the sea site is given by:

$$AEP = A\eta \sum_{x=1}^{V} P_{absorbed}(x)T_h(x)$$
 (25)

where $\eta = 0.7$ is the power conversion efficiency (Chozas et al., 2014), and A = 0.9 accounts for the WEC availability, considering

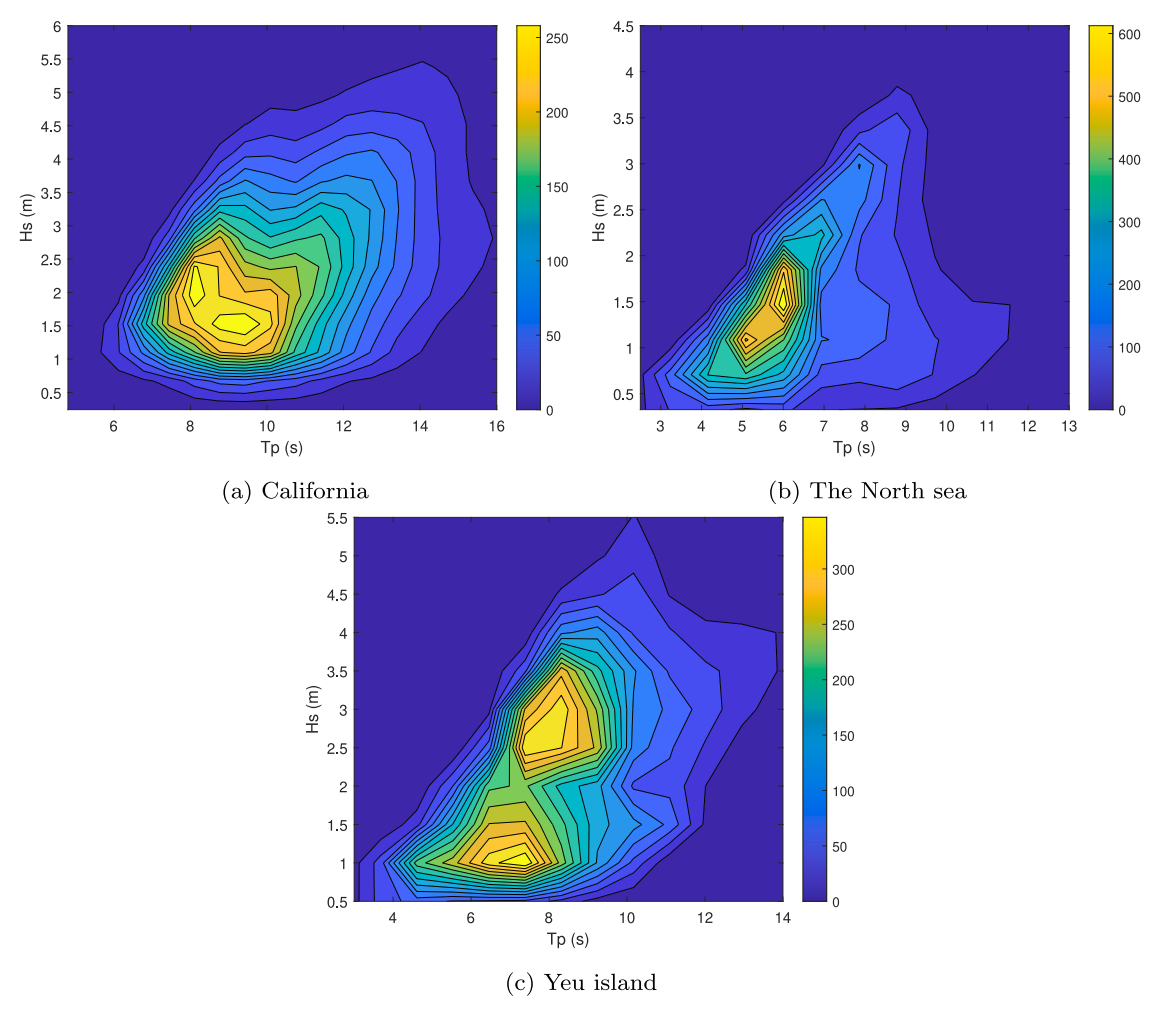


Fig. 4. Scatter diagram of the annual occurrence of hours of different sea states for considered sea sites.

maintenance (Kramer et al., 2011). T_h represents total operational hours for each sea state x, with V denoting the number of wave states.

Another insightful indicator in the techno-economic analysis is the capacity factor (CF) (Rusu and Onea, 2018), which can be calculated as

$$CF = \frac{AEP}{P_{rated} \times 8760} \tag{26}$$

where "8760" is the amount of total hours per year. Hence, CF implies the ability of the WEC to achieve designed power capacity at the specific sea site.

2.6. Fatigue damage estimation

This study evaluates the fatigue damage experienced by the PTO rod under realistic wave climates. The PTO force results obtained from the three different WEC dynamic models are used as inputs for the fatigue damage assessment. Various approaches have been proposed for predicting the fatigue damage of offshore structures (Muñiz-Calvente et al., 2022). Given a time history of the loads, TD methods, such as the widely used rain-flow counting method, can be employed to characterize load cycle distributions (Amzallag et al., 1994; Kebir et al., 2021; Quigley et al., 2016). While this method is considered highly accurate for fatigue damage estimation, it requires a substantial amount of time-dependent load data and is computationally expensive. Alternatively, several FD methods, including the Narrow-band method, Jiao-Moan method, and Dirlik method, can statistically describe load cycle distributions based on the load spectrum (Dirlik and Benasciutti, 2021; Jimenez-Martinez, 2020). Among these, the Dirlik method

has been shown to provide highly accurate fatigue damage estimates comparable to those obtained using the rain-flow method, particularly in the context of WECs (Martinez-Puente et al., 2023). Therefore, the Dirlik method is adopted in this study for fatigue estimation across all three numerical models. While different fatigue estimation methodologies may be more suitable for specific scenarios, a detailed discussion of these methodologies is beyond the scope of this study.

Based on the calculated PTO loads by different WEC dynamic models, the stress exerted on the PTO rod is calculated as

$$s = \frac{F_{pto}}{3 \times A_{rod}} \tag{27}$$

where s is the stress; A_{rod} embodies the cross-sectional area of the three PTO rods. The PSD of the stress on the rod can be calculated as

$$G(f) = \frac{1}{2} \frac{|\hat{s}(f)|^2}{\Delta f}$$
 (28)

where G(f) is the PSD at the frequency component f, and f denotes the frequency in Hertz. Then, the statistical moments of the stress PSD are expressed as

$$\lambda_i = \int_0^\infty f^i G(f) \, df \tag{29}$$

where λ_i means the i_{th} spectral moment of the stress PSD. Referring to the Dirlik method (Dirlik and Benasciutti, 2021), the probability density function (PDF) of the stress range at S can be estimated as an empirical formula:

$$p(S) = \frac{\frac{D_1}{Q} \exp\left(-\frac{Z}{Q}\right) + \frac{D_2 Z}{R^2} \exp\left(\frac{-Z^2}{2R^2}\right) + D_3 Z \exp\left(\frac{-Z^2}{2}\right)}{2\sqrt{\lambda_0}}$$
(30)

Table 3 Material constants of cast iron used in the PTO rod (Li et al., 2017).

Parameters	Quantities
Ultimate strength S_{ut}	500 MPa
Fatigue strength S_{fa}	250 MPa
Fatigue exponent k	0.13

where D_1 , D_2 , D_3 , R, Z, Q, γ and x_m are fitting parameters, and their identification can be referred to Appendix B.

With the PDF of stress ranges derived, the stress fatigue damage rate can be obtained following Miner's law (Dirlik and Benasciutti, 2021) as

$$d = \int_0^\infty \frac{f_m}{N_f(S)} p(S) \, dS \tag{31}$$

where d is the fatigue stress damage rate, which indicates the damage per unit time in seconds; f_m is the mean frequency and updated at each sea state, $N_f(S)$ embodies the number of cycles to failure at S, as described in the S–N curve:

$$N_f(S) = \left(\frac{S}{S_{ut}}\right)^{-k} \tag{32}$$

where S_{ut} is the ultimate strength, and k are material fatigue parameters.

Substituting (32) to (31) gives:

$$d = f_m \int_0^\infty \left(\frac{S}{S_{ut}}\right)^{-k} p(S) \, dS \tag{33}$$

Then, the annual accumulated fatigue damage of the PTO rod at one sea site can be as

$$D = \sum_{x=1}^{V} d(x)T_h(x) \times 3600 \tag{34}$$

Subsequently, the fatigue life of the PTO rod in years is:

$$L = \frac{1}{D} \text{ (years)} \tag{35}$$

In this study, the rod material is considered as medium-carbon steel, and the relevant material constants for the fatigue property are given in Table 3.

3. Results

3.1. Verification of WEC dynamic models

Verifying the three numerical models is a crucial first step. The dynamic responses of the WEC predicted by each model are compared to assess their consistency. Initial simulations are conducted in a mild sea state, where the models are expected to yield identical results. The PSD of the WEC velocity and the intrinsic impedance of the WEC calculated by the three models are compared. The intrinsic impedance $Z(\omega)$ is frequency-dependent and calculated as

$$\hat{Z}(\omega) = \frac{\hat{F}_{e}(\omega)}{\mathrm{i}\omega\hat{z}(\omega)} \tag{36}$$

Regarding the TD model, $\hat{F}_e(\omega)$ and $\hat{z}(\omega)$ are obtained by applying FFT to the time-series data.

Figs. 5 and 6 present the derived PSD of the velocity and the impedance of the WEC. In the simulation, the significant wave height and the peak period are defined as 0.26 m and 8.2 s, and the PTO damping R_{pto} is selected following (19). It is visible that these figures demonstrate strong agreement among the three models, confirming their correct implementation.

The standard deviation of the WEC velocity across a range of peak periods is shown in Fig. 7, in which two different significant wave heights are considered. As shown in Fig. 7(a), the discrepancies between the standard deviation of the WEC velocity calculated by

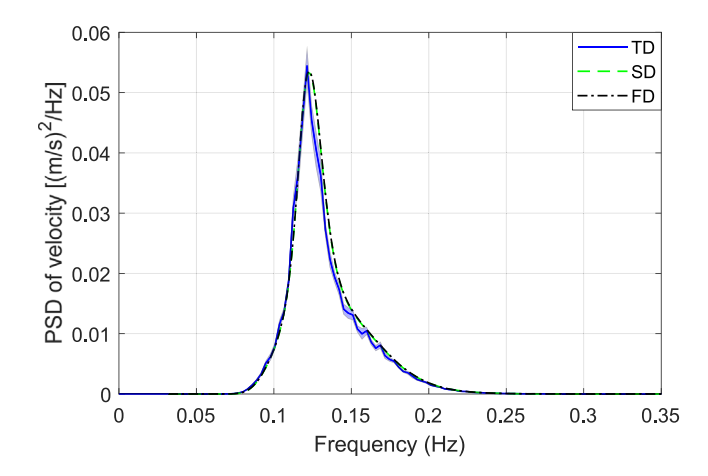
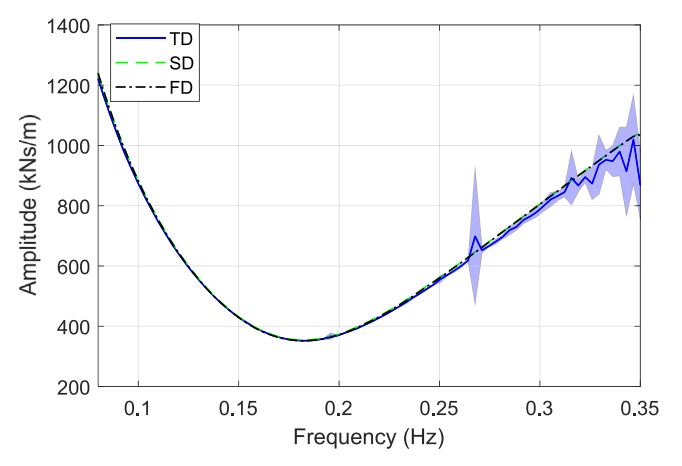
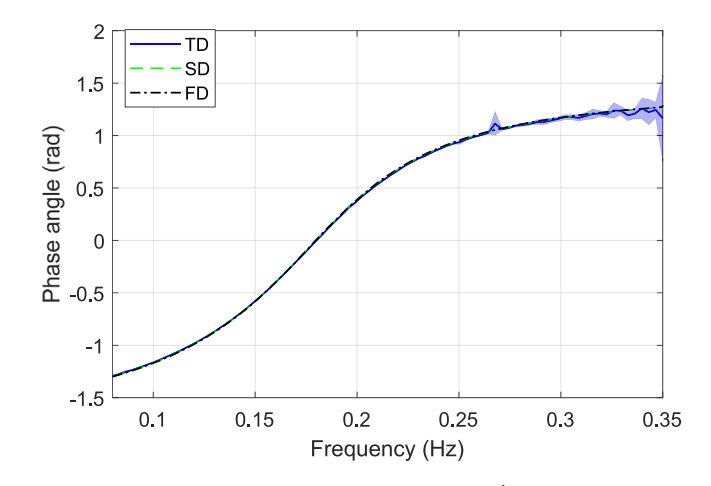


Fig. 5. The power spectral density of the velocity of the WEC ($H_s=0.26~{\rm m}$ and $T_p=8.2~{\rm s};~R_{pto}=340~{\rm kNs/m}$). The shaded area is used to represent the standard deviation of multiple TD simulations.



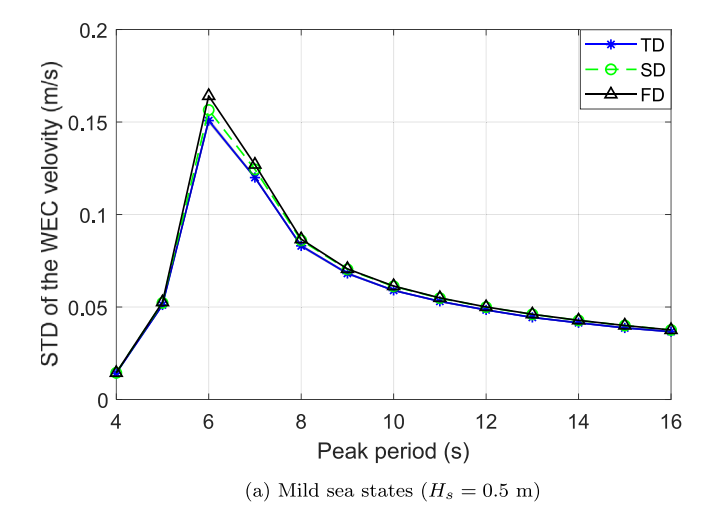
(a) Impedance amplitude $|\hat{Z}(\omega)|$



(b) Impedance phase angle $\angle \hat{Z}(\omega)$

Fig. 6. The intrinsic impedance of the WEC derived by different numerical models ($H_s = 0.26$ m and $T_p = 8.2$ s; $R_{plo} = 340$ kNs/m). The shaded area is used to represent the standard deviation of multiple TD simulations.

the three numerical models appear negligible in mild sea states. As the significant wave height increases, nonlinear effects become more pronounced. Fig. 7(b) illustrates the standard deviation of the WEC velocity in more energetic sea states, where the significant wave height



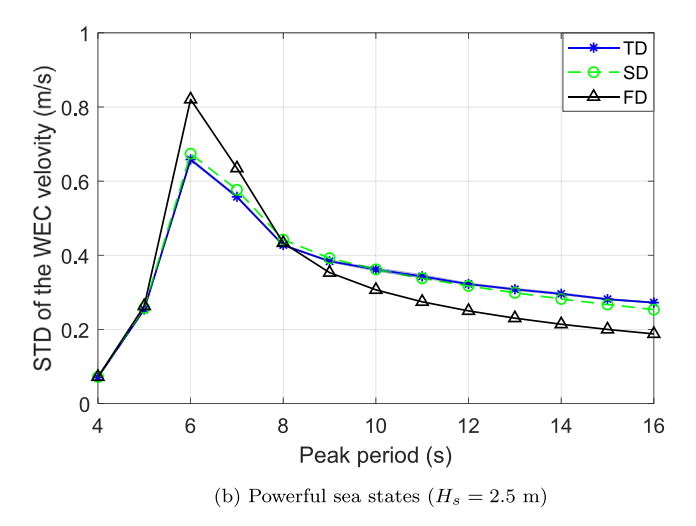


Fig. 7. The standard deviation of the WEC velocity at various peak periods.

is 2.5 m. Here, deviations between the FD and TD models become noticeable, with the FD model exhibiting a relative error of up to 20% at a peak period of 6 s. In contrast, the SD model closely aligns with the nonlinear TD model. This outcome is expected, as the SD model incorporates nonlinear effects through statistical linearization, making it inherently more accurate than the FD model in energetic wave conditions.

3.2. On the power performance

This section examines how the choice of numerical WEC dynamic model affects power performance estimation. The power matrices obtained from the three models are presented in Figs. 8, 9, and 10. All three models exhibit similar trends in power absorption across different sea states. Specifically, they capture the general pattern of power increasing with the peak period before declining beyond a certain threshold. The maximum absorbed power occurs at a significant wave height of 5 m and a peak period of approximately 8–9 s in all cases.

At mild sea states (significant wave height below 1 m), the three models yield nearly identical results, with negligible discrepancies. However, as wave height increases, the FD model begins to diverge from the TD model due to intensified nonlinear effects. In contrast, the SD model remains closely aligned with the TD model in power absorption estimates. Notably, the FD model significantly overestimates the maximum power compared to the other two models. Specifically,

it predicts a peak power of 233.6 kW, while the SD and TD models estimate 130.7 kW and 127 kW, respectively. This results in a substantial relative error of approximately 84% for the FD model compared to the TD model. By contrast, the SD model maintains a relative error of no more than 9% across all sea states, suggesting that the SD model demonstrates a strong capability for accurately assessing WEC power absorption.

3.3. On the techno-economic metrics

The impacts of the numerical modeling selection on the techno-economic evaluation are demonstrated in this section. The discrepancies in power performance estimation among the three numerical models inevitably lead to deviations in the techno-economic assessment of the WEC. Table 4 presents the AEP values for the WEC at different sea sites, as estimated by the three models. The FD model consistently overestimates the AEP relative to the reference TD model, with this overestimation observed across all examined locations.

As shown in Table 5, the relative error of the FD model compared to the TD model ranges from 19.5% to 29.8%, depending on the sea site. The highest relative error occurs at Yeu Island, followed closely by the California sea site. This trend can be attributed to the frequent occurrence of powerful sea states at these locations, where the FD model exhibits reduced accuracy due to its inability to capture nonlinear effects, as demonstrated in previous analyses. Comparatively, the SD model delivers only a slight overestimation relative to the TD model, with relative errors ranging from 3.6% to 6.6%.

Tables 6 and 7 show the CF estimated by the three models and the corresponding deviations of the SD and FD models compared to the results obtained by the TD model. Clearly higher values of the CF are obtained by the FD model compared to those by the TD model, and the deviation varies from 29.7% to 48.0%. The SD model performs much better than the FD model, with overestimating the CF values by maximally 6.47%. This further supports the SD model's capability as a balanced approach, offering improved accuracy over the FD model while maintaining computational efficiency.

The LCOE is a widely used metric that comprehensively reflects the economic feasibility of a WEC design at a given sea site. In this study, the LCOE of the WEC is evaluated across the three considered sea sites using different WEC dynamic models, as shown in Table 8. Results indicate a strong dependence of LCOE on wave resource. According to the TD model, the lowest LCOE is observed at the California sea site, with a value of 0.5316 Euros/kWh, while the highest LCOE is found in the North Sea, reaching 1.5568 Euros/kWh. These variations not only imply differences in wave power across locations but also highlight the impact of WEC design suitability, such as floater size and geometry, on site-specific wave characteristics. When comparing LCOE estimates from the three numerical models, it is evident that all models capture the general trend of LCOE variation with wave resources. For example, all three models consistently identify the North Sea as having the highest LCOE and California as having the lowest. However, in terms of absolute values, the FD model significantly underestimates LCOE compared to the TD model. For instance, at Yeu Island, the FD model estimates an LCOE of 0.5721 Euros/kWh, whereas the TD model gives a much higher estimate of 0.8552 Euros/kWh, resulting in a relative error of 33.1%. As a comparison, the SD model demonstrates strong agreement with the TD model across all sea sites. As shown in Table 9, the maximum relative error between the SD and TD models is only 6.2%, reinforcing the SD model's suitability as a more reliable alternative to the FD model for techno-economic assessments.

3.4. On the fatigue damage

The stress fatigue damage rate d on the PTO rod is estimated using the three different WEC dynamic models across various sea states. The results are presented in Figs. 11, 12, and 13. A comparison of these

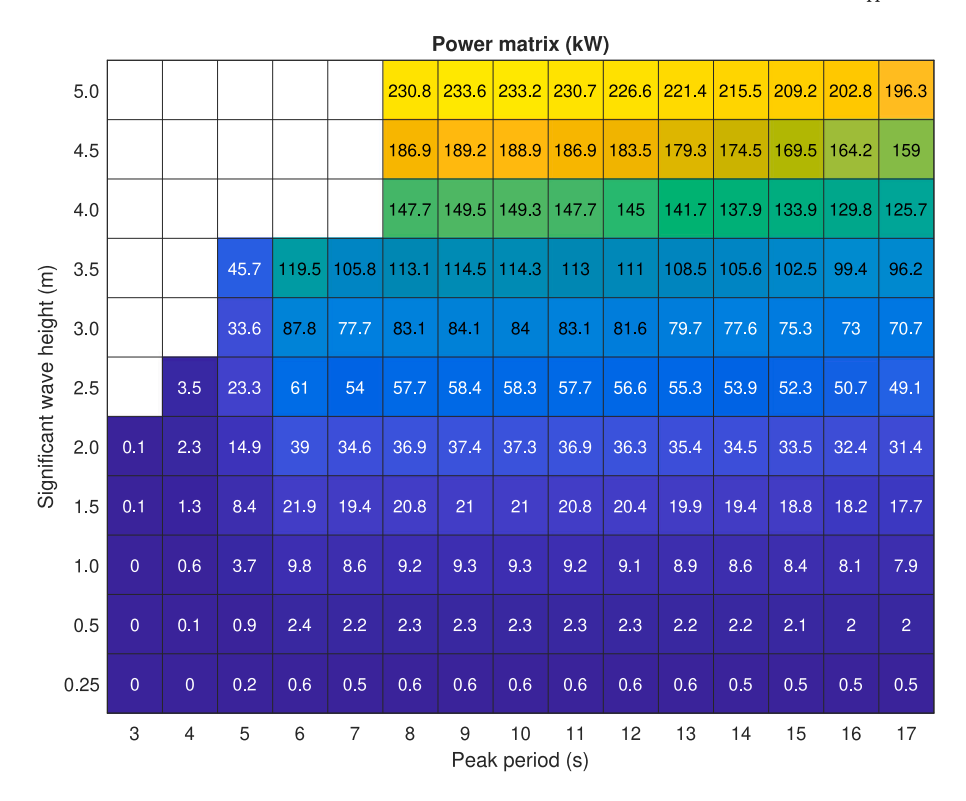
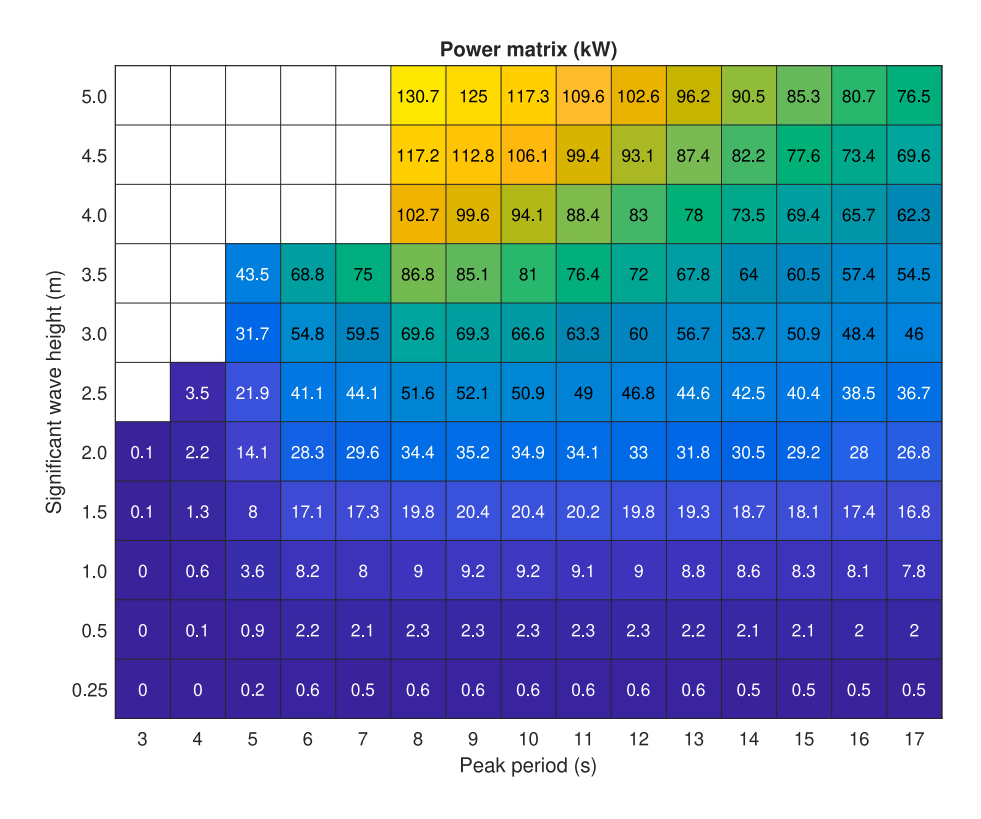


Fig. 8. Power matrix estimated by the FD model.



 $\textbf{Fig. 9.} \ \ \textbf{Power matrix estimated by the SD model}.$

figures reveals significant discrepancies between the FD model, the SD and TD models in estimating the fatigue damage rate. Firstly, the SD and TD models predict the highest fatigue damage rate at a sea state with the same peak period of approximately 8 s, whereas the FD model estimates the maximum fatigue damage rate at a peak period

of 17 s, indicating a substantial deviation. In addition, at powerful sea states, the FD model predicts fatigue damage rates several orders-of-magnitude higher than those estimated by the SD and TD models. Specifically, the maximum fatigue damage rate predicted by the TD model is approximately 2.0×10^{-6} , while the FD model estimates a

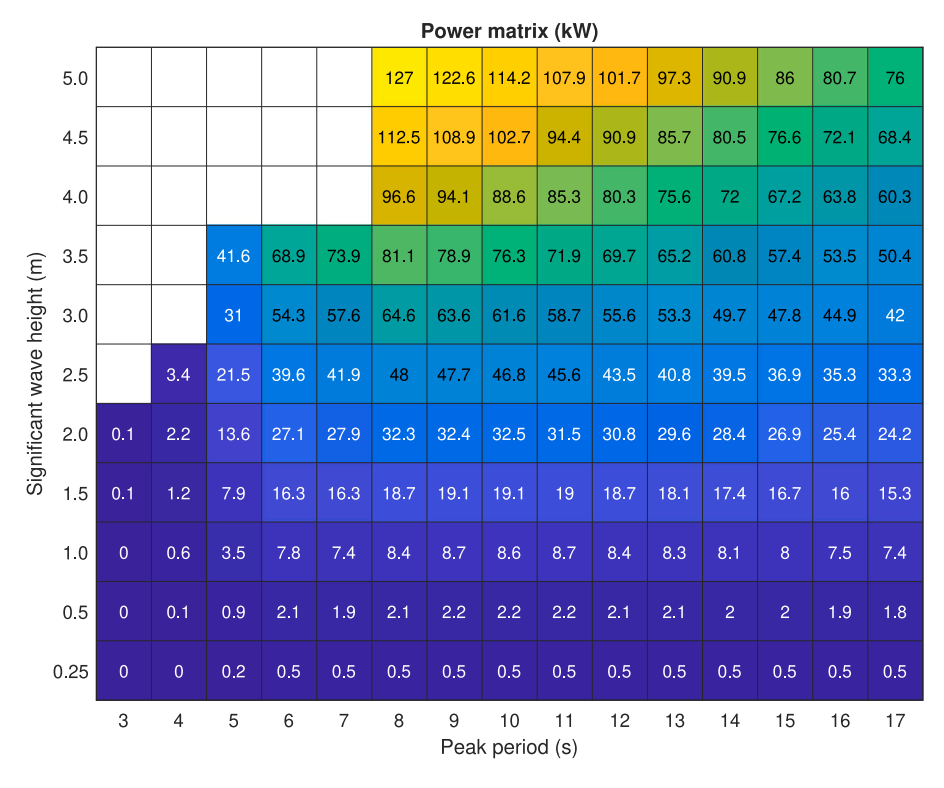


Fig. 10. Power matrix estimated by the TD model.

Table 4
The values of the AEP estimated by different WEC dynamic models.

	FD modeling (MWh)	SD modeling (MWh)	TD modeling (MWh)
Yeu island	283.2	196.4	189.5
North Sea	135.1	110.7	104.1
California	432.5	324.9	304.8

Table 5
The deviation of the AEP estimated by the FD and SD model to the TD model.

	FD modeling	SD modeling
Yeu island	49.5%	3.6%
North Sea	29.8%	6.3%
California	41.9%	6.6%

Table 6
The values of the CF estimated by different WEC dynamic models.

FD modeling	SD modeling	TD modeling
12.8%	8.97%	8.65%
6.16%	5.05%	4.75%
19.8%	14.8%	13.9%
	12.8% 6.16%	12.8% 8.97% 6.16% 5.05%

 $\begin{tabular}{ll} \textbf{Table 7} \\ \textbf{The deviation of the CF estimated by the FD and SD model to the TD model.} \\ \end{tabular}$

	FD modeling	SD modeling
Yeu island	48.0%	3.70%
North Sea	29.7%	6.32%
California	42.5%	6.47%
•		

significantly higher value of around 6.5×10^{-4} . This discrepancy arises because the linear FD model does not account for PTO force saturation, leading to an overestimation of PTO forces in high-energy wave conditions where saturation effects become pronounced. Conversely, the SD model effectively captures the variation trends of fatigue damage rates across different sea states. Both the SD and TD models indicate that

the fatigue damage rate generally increases with peak period up to 8 s before decreasing at longer peak periods. Moreover, the maximum fatigue damage rate predicted by the SD model is 7.0×10^{-7} , which is approximately half of the corresponding value from the TD model, suggesting that the SD model provides a reasonable approximation while still underestimating fatigue damage. Fig. 14 further illustrates the comparison of the three models in estimating fatigue damage rate. It is observed that at low significant wave heights, all three models provide similar estimates. However, as the significant wave height increases, the FD model diverges considerably from the SD and TD models, reinforcing its reduced accuracy in highly nonlinear conditions.

Table 10 presents the annually accumulated fatigue damage D on the PTO rods. It can be seen that the FD model gives unrealistically higher accumulated fatigue damage than that of the TD modeling. For instance, the annually accumulated fatigue damage at the Yeu island estimated by the TD model is 0.0365 while it is 8.5646 by the FD model, with a difference of over 200 times. In the sea site in California, the estimation difference could even reach around 690 times. This also implies that the fatigue life of the PTO rod is significantly underestimated when using the FD model to predict the WEC dynamics. Specifically, according to the TD modeling, the fatigue life at the Yeu island is around 27 years, while it is 0.11 years based on the estimation of the FD modeling. The SD model also exhibits deviations from the TD model. The accumulated fatigue damage estimated by the SD model is lower than that of the TD modeling. This implies the overestimation of the fatigue life by the SD model. However, the SD model could roughly approximate the fatigue damage and fatigue life with regard to the results of the TD modeling. The maximum discrepancy of the

Table 8

The values of the LCOE estimated by different WEC dynamic models.

	FD modeling (Euros/kWh)	SD modeling (Euros/kWh)	TD modeling (Euros/kWh)
Yeu island	0.5721	0.8251	0.8552
North Sea	1.1996	1.4642	1.5568
California	0.3746	0.4986	0.5316

 $Table \ 9 \\ The \ deviation \ of \ the \ LCOE \ estimated \ by \ the \ FD \ and \ SD \ model \ to \ the \ TD \ model.$

	FD modeling	SD modeling
Yeu island	33.1%	3.5%
North Sea	22.9%	5.9%
California	29.5%	6.2%

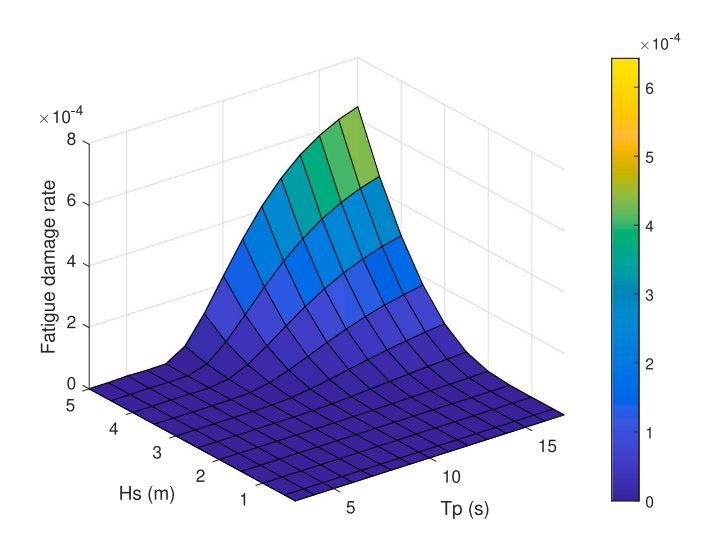


Fig. 11. The fatigue damage rate at various sea states, estimated based on the FD model.

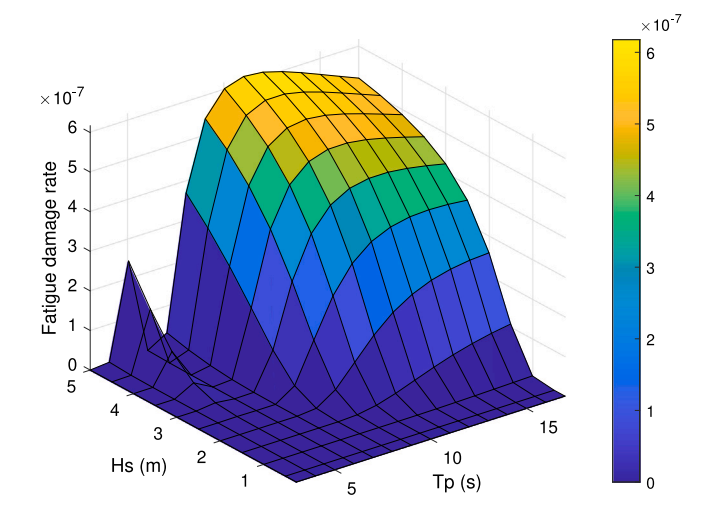
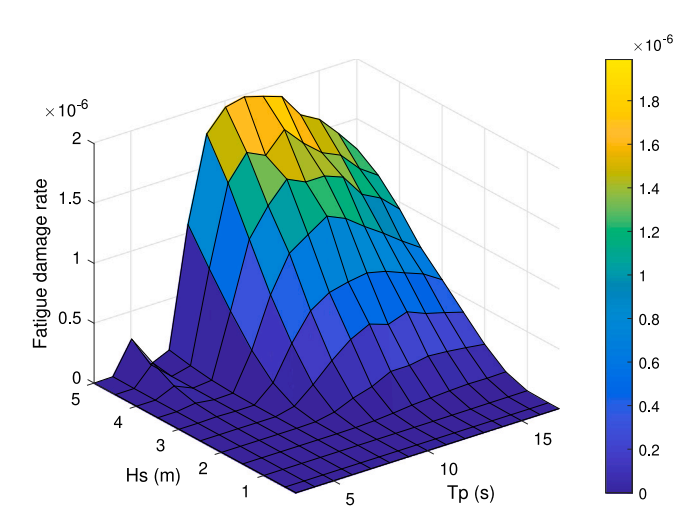


Fig. 12. The fatigue damage rate at various sea states, estimated based on the SD model.

estimated accumulated fatigue damage by the SD model occurs at Yeu island, where the value is 0.0365 and 0.0137 comes from the TD and SD models, respectively. This difference is maintained less than 3 times, which is much improved compared to the linear FD model. At all the



 ${f Fig.~13.}$ The fatigue damage rate at various sea states, estimated based on the TD model.

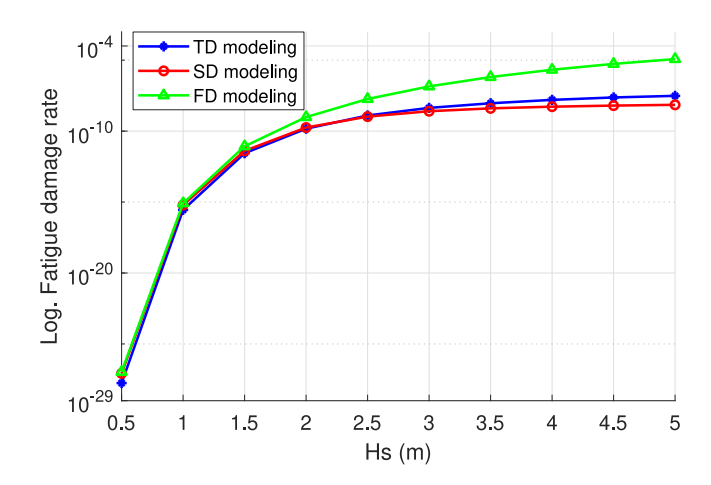


Fig. 14. The comparison of the fatigue damage rate estimated based on different WEC dynamic models $(T_p=9s)$.

Table 10

The annually accumulated fatigue damage estimated by different WEC dynamic models.

	FD modeling	SD modeling	TD modeling
Yeu island	8.5646	0.0137	0.0365
North Sea	2.8700	0.0076	0.0164
California	158.14	0.0961	0.2272

sea states, the SD model gives nearly the same order-of-magnitude estimation as the TD modeling approach.

3.5. Computational efficiency

On top of modeling fidelity, computational efficiency is an important and practical factor, particularly in the early design stages, where numerous design iterations and optimizations are required. The three WEC dynamic models exhibit significantly different computational efficiencies. To quantify these differences, the computational time required

Table 11Computational time of different numerical modeling approaches for one simulation case (the sea state is specified as such with a significant wave height of 2 m and a peak period of 6 s).

0 1 1	
Numerical models	Computational time
FD model	1.4×10^{-2} s
SD model	3.4×10^{-1} s
TD model	375.2 s (10-runs)

by each model is identified and compared, as presented in Table 11. All simulations are performed on the same computing machine equipped with an Intel i7/2.80 GHz processor to ensure a fair comparison. As shown in Table 11, the FD model demonstrates the highest computational efficiency, requiring negligible computational time. The SD model, while incorporating nonlinear effects through statistical linearization, requires approximately 10 times more computational time than the FD model. Comparatively, the TD model, implemented via WEC-Sim, demands significantly greater computational resources, requiring over 1000 times the computational time of the SD model. These results highlight the distinct advantage of the SD model: it effectively accounts for nonlinear effects while maintaining significantly higher computational efficiency compared to the TD model. This makes the SD approach particularly suitable for early-stage design exploration and optimization processes, where computational cost is a critical consideration.

4. Discussion

It should be noted that all numerical modeling approaches, including the nonlinear TD model presumed the "true reference" in this study, are associated with varying levels of underlying limitations. First, all three models are fundamentally based on linear potential flow theory. While selected weakly nonlinear effects are incorporated into the SD and TD models, the hydrodynamic coefficients, namely, excitation force, radiation damping, and added mass, are derived using the linear potential flow-based solver Nemoh. Secondly, the wave inputs used throughout this study are consistently assumed to be unidirectional Airy waves. As a result, the simulation results are theoretically valid only for relatively small to moderate unidirectional wave conditions. Thirdly, the statistical linearization used in the SD model is based on the assumption that the WEC system response follows a Gaussian process. This assumption remains valid for Airy waves and relatively linear regimes of WEC systems. However, as the nonlinearity of the system increases, the Gaussian assumption becomes less valid, resulting in reduced accuracy of the SD model (Folley and Whittaker, 2010; Tan et al., 2022b). Fourthly, the incorporation of nonlinear phenomena into the Cummins-equation-based TD model involves certain idealizations. For example, viscous effects are represented using an empirical Morison drag term. While this term provides a practical and efficient means to model effects induced by viscous flow, it is suitable mainly for mild sea states and may not accurately capture extreme conditions such as wave breaking, slamming, or other complex viscous flow phenomena (Folley, 2016). Fifthly, only a passive PTO system is considered in this work for simplification. The use of an optimal controller or other advanced control strategies would, on the one hand, lead to different outcomes in the performance evaluations. On the other hand, the implementation of such controllers, particularly optimal control strategies that induce higher motion amplitudes of the WEC, would also increase the nonlinearities of the WEC system (Faedo et al., 2017). As a consequence, it would result in a greater deviation of the linear FD model from the SD and nonlinear TD models.

The implementation of numerical models inevitably introduces uncertainties into the simulation results. First, uncertainties in the computation of hydrodynamic coefficients may arise from factors such as mesh quality, frequency resolution, range of frequencies considered, and the choice of hydrodynamic solver (Raghavan et al., 2024; Penalba et al., 2017b). In this study, this particular source of uncertainty is eliminated, as all three models share an identical set of hydrodynamic coefficients. However, in general, the hydrodynamic analysis could introduce a noticeable source of potential uncertainty in WEC performance evaluation. Secondly, the SD model involves an iterative solution procedure to derive the standard deviation of the unknown responses, where the definition of the convergence tolerance introduces another layer of uncertainty (Folley and Whittaker, 2013; Tan et al., 2023; Folley, 2016). Thirdly, the state-space approximation used in the TD model to evaluate the radiation convolution integral also introduces uncertainty. Several methods can be used for this approximation, such as the Prony method, time-domain identification, and frequency-domain identification, each with differing theoretical bases and accuracy levels (Tom et al., 2015). Furthermore, the number of additional states used in the approximation can affect the accuracy of simulation outputs (Folley, 2016). Fourthly, uncertainties arise from the choice of the numerical integration algorithm to solve the system of differential equations in the TD model. Various solvers are available and associated with different principles, including the fourth-order Runge-Kutta method, Backward Euler method, and Crank-Nicolson method (Folley, 2016). The choice of the solution algorithm, along with parameters such as time step size and total simulation duration, can influence the accuracy and stability of the results. Additionally, when modeling WEC responses under irregular wave conditions, each TD simulation may exhibit variability due to the stochastic nature of the wave input. Typically, a random phase is assigned to each frequency component to construct the wave time series. Consequently, multiple simulation runs are often required for a given sea state to increase the statistical sample size and reduce random errors in the derived performance metrics. In this context, both the number of simulation runs and the duration of each run contribute to the overall modeling uncertainty (Kvittem and Moan, 2015; Gao et al., 2023). In the current work, all modeling specifications or justifications related to these sources of uncertainty have been provided in the descriptions of the respective modeling approaches. Nonetheless, it should be acknowledged that these uncertainties, although potentially limited in magnitude, can influence the simulation outcomes and the resulting systematic performance evaluations in ways that extend beyond the scope of factors considered in this benchmarking study.

5. Conclusion

In this paper, a benchmark study of three predominant numerical WEC dynamic models is conducted to assess their applicability in evaluating the systematic performance of a WEC system. The three numerical modeling approaches include the FD modeling, SD modeling, and the WEC-Sim model, which represents the TD modeling approach. The systematic performance evaluation of the WEC is carried out across three key aspects:

- Power Performance: The power absorption under varying sea states, which is formatted as a power matrix.
- Techno-Economic Performance: Assessment of key indicators reflecting the cost-effectiveness of the WEC, including the AEP, the CF and the LCOE.
- Fatigue Damage Estimation: Prediction of fatigue damage on the PTO connection rods, which is crucial for long-term reliability and durability of the WEC.

Towards a comprehensive and realistic benchmarking, multiple sea sites from different geographical locations are considered in the performance evaluation. Additionally, the computational efficiency of the three models is identified and compared. It should be clearly acknowledged that these conclusions are specific to this particular study, including the chosen WEC type, implementation methods of numerical

models, underlying assumptions, environmental inputs, performance estimation methods, and other related factors. Any generalization of the conclusions should be approached with caution, taking into account the variability of affecting factors as addressed in Section Discussion. Nevertheless, the main takeaways derived from the current benchmarking study are drawn below.

Firstly, the FD, SD, and TD models are all applicable for estimating power performance, techno-economic performance, and fatigue damage. However, due to variations in modeling fidelity, discrepancies are observed in the evaluation results obtained from these models. Notably, the magnitude of these discrepancies varies significantly depending on the specific performance metric being assessed. In this regard, selecting an appropriate numerical modeling approach is crucial for ensuring a reasonable and accurate performance evaluation of WECs. The selection of the numerical model should be aligned with the performance metric under investigation, aiming for a reasonable performance evaluation of WECs. Furthermore, it should be noted that the different models are appropriate depending on the task at hand. For instance, SD and FD models are more useful than the TD model with regard to understanding design trade-offs, control strategies, etc. Comparatively, TD models are more preferable for revealing higher-fidelity aspects.

Secondly, regarding the power performance estimation, the three WEC dynamic models converge well at relatively mild sea states. For this specific WEC, with the increase of the significant wave height, the results of the FD model noticeably deviate from those of the TD model, and the maximum relative error reaches 84%. Comparatively, the power estimation of the SD model closely aligns with that of the TD model, in which the maximum error is less than 9% across all the considered sea states in the power matrix. Furthermore, it should be noted that the dependence of the nonlinearity of WECs is also related to other factors. These discrepancies between the models could exhibit different trends in the significant wave height with varied WEC geometry or control strategies.

Thirdly, both the FD model and the SD model provide more optimistic estimations of the AEP, the CF and the LCOE compared to the reference TD model at the three considered sea sites. Specifically, the FD model overestimates the AEP by 29.8% to 49.5%, overestimates the CF by 29.7% to 48.0% and underestimates the LCOE by 22.9% to 33.1%, depending on the sea site. In contrast, the SD model demonstrates significantly higher accuracy relative to the TD model, with deviations ranging from 3.6% to 6.6% for the AEP, 3.7% to 6.47% for the CF and 3.5% to 6.2% for the LCOE, respectively.

Fourthly, due to the lack of nonlinear elements, particularly the force saturation effect, the FD model exhibits severe weakness in fatigue damage estimation. Compared to the nonlinear TD model, the FD model is unable to capture the variations in fatigue damage rate across different sea states. The accumulated fatigue estimated by the FD model is around 175 to 690 times larger than the values estimated by the TD model, depending on the sea site. This overestimation suggests that the fatigue life of the PTO rods would be significantly underestimated if the FD model were used. As a comparison, the SD model provides a more reasonable approximation of fatigue damage. It successfully captures the trends in fatigue damage rate variations with changing sea states, and the sea state associated with the highest fatigue damage rate predicted by the SD model aligns with that identified by the TD model. Furthermore, the accumulated fatigue damage estimated by the SD model is nearly of the same order-of-magnitude as the TD modeling estimation across all three sea sites.

Finally, the difference in computational time between the three WEC dynamic models appears remarkable. As identified in this study, the TD model, implemented via WEC-Sim, requires computational resources over a thousand times greater than the SD model, which in turn is more than 20 times slower than the FD model. In practice, the computational efficiency would inevitably impact the selection of the numerical models when carrying out the performance evaluation of WECs. However, it should be acknowledged that the nonlinear TD

model is expected to deliver more reliable evaluation results than the other two models because of its inherently being associated with higher modeling fidelity. Hence, the TD model should be prioritized over the SD and FD models if the computational resource or time schedule allows. As an alternative, the SD model perceives a good compromise between the computational time and the accuracy of the performance evolution. Particularly, the SD model presents limited discrepancies in the evaluation of the power performance, the AEP, and the LCOE. It is highly suited for early-stage design and optimization of WECs, requiring a huge amount of numerical simulation iterations. However, the FD model is an appropriate option to preliminarily characterize the dynamic response and power absorption of WEC to ocean waves, while it demonstrates sufficient applicability to rather linear regimes, such as less powerful waves and mild operation conditions.

CRediT authorship contribution statement

Jian Tan: Writing – review & editing, Writing – original draft, Visualization, Validation, Supervision, Software, Methodology, Investigation, Formal analysis, Data curation, Conceptualization. Ryan G. Coe: Writing – review & editing, Visualization, Validation, Supervision, Methodology, Investigation, Formal analysis, Conceptualization. George Lavidas: Writing – review & editing, Supervision, Resources, Project administration, Methodology, Funding acquisition, Conceptualization.

Declaration of competing interest

The authors declare that they have no known competing financial interests or personal relationships that could have appeared to influence the work reported in this paper.

Acknowledgments

This work was supported by the US Department of Energy's Water Power Technologies Office. Sandia National Laboratories is a multimission laboratory managed and operated by National Technology and Engineering Solutions of Sandia, LLC., a wholly owned subsidiary of Honeywell International, Inc., for the U.S. Department of Energy's National Nuclear Security Administration under contract DE-NA0003525. This paper describes objective technical results and analysis. Any subjective views or opinions that might be expressed in the paper do not necessarily represent the views of the U.S. Department of Energy or the United States Government.

This research was also funded by the Dutch Research Council (Nederlandse Organisatie voor Wetenschappelijk Onderzoek-NWO) with Project No. EP.1602.22.001 and the CETPartnership, the Clean Energy Transition Partnership under the 2022 CETPartnership joint call for research proposals, co-funded by the European Commission (GAN° 101069750) Project No. CETP-2022-00127.

Appendix A. Derivation of statistical linearization in SD modeling

The fundamental principle of the statistical linearization is to find a linear coefficient which is expected to dissipate the same amount of energy with the exact nonlinear effect in a random vibration system (Roberts and Spanos, 2003; Folley and Whittaker, 2010). Defining a generic nonlinear function F_{non} :

$$F_{non} = g(u) \tag{A.1}$$

where u is the input variable and g is a nonlinear function. Its linear approximation, $f_a(u)$, is given by

$$f_e(u) = Nu + M \tag{A.2}$$

where N and M are quasi-linear coefficients. The linearization error is

$$\epsilon = g(u) - Nu - M \tag{A.3}$$

Minimizing the expected squared error, $\langle \epsilon^2 \rangle$, where $\langle \cdot \rangle$ denotes expectation, requires

$$\frac{\partial}{\partial N}\langle \epsilon^2 \rangle = 0, \quad \frac{\partial}{\partial M}\langle \epsilon^2 \rangle = 0$$
 (A.4)

Solving (A.4) gives

$$N = \frac{\langle ug(u)\rangle}{\langle u^2\rangle}, \quad M = \langle g(u)\rangle \tag{A.5}$$

It can be deduced that M would be zero if the statistical contribution of the function g(u) is zero-mean.

Appendix B. Fitting parameters identification in Dirlik method

In Dirlik method, the PDF for each stress range can be derived based on an empirical formula (30), in which a set of fitting parameters is needed as the input. As detailed in Dirlik and Benasciutti (2021), the fitting parameters can be calculated as

$$D_{1} = \frac{2(x_{m} - \gamma^{2})}{1 + \gamma^{2}}$$

$$D_{2} = \frac{1 - \gamma - D_{1} + D_{1}^{2}}{1 - R}$$

$$D_{3} = 1 - D_{1} - D_{2}$$

$$Z = \frac{S}{2\sqrt{\lambda_{0}}}$$

$$Q = \frac{1.25(\gamma - D_{3} - D_{2}R)}{D_{1}}$$

$$R = \frac{\gamma - x_{m} - D_{1}^{2}}{1 - \gamma - D_{1} + D_{1}^{2}}$$

$$\gamma = \frac{\lambda_{2}}{\sqrt{\lambda_{0}\lambda_{4}}}$$

$$x_{\lambda} = \frac{\lambda_{1}}{\lambda_{0}} \sqrt{\frac{\lambda_{2}}{\lambda_{4}}}$$
(B.1)

References

- Alday Gonzalez, M., Lavidas, G., 2024. The ECHOWAVE hindcast.
- Amini, E., Asadi, R., Golbaz, D., Nasiri, M., Naeeni, S.T.O., Majidi Nezhad, M., Piras, G., Neshat, M., 2021. Comparative study of oscillating surge wave energy converter performance: A case study for southern coasts of the Caspian sea. Sustainability 13 (19), 10932.
- Amzallag, C., Gerey, J., Robert, J.L., Bahuaud, J., 1994. Standardization of the rainflow counting method for fatigue analysis. Int. J. Fatigue 16 (4), 287–293.
- Babarit, A., Hals, J., Muliawan, M.J., Kurniawan, A., Moan, T., Krokstad, J., 2012. Numerical benchmarking study of a selection of wave energy converters. Renew. Energy 41, 44–63.
- Ballard, B., Yu, Y.-H., Van Rij, J., Driscoll, F., 2020. Umbilical fatigue analysis for a wave energy converter. In: International Conference on Offshore Mechanics and Arctic Engineering, vol. 84416, American Society of Mechanical Engineers, V000T09A028
- Bonfanti, M., Giorgi, G., 2022. Improving computational efficiency in WEC design: Spectral-domain modelling in techno-economic optimization. J. Mar. Sci. Eng. 10 (10), 1468.
- Bosma, B., Zhang, Z., Brekken, T.K., Özkan-Haller, H.T., McNatt, C., Yim, S.C., 2012. Wave energy converter modeling in the frequency domain: A design guide. In: 2012 IEEE Energy Conversion Congress and Exposition. ECCE, IEEE, pp. 2099–2106.
- Chandrasekaran, S., Sricharan, V., 2021. Numerical study of bean-float wave energy converter with float number parametrization using WEC-sim in regular waves with the levelized cost of electricity assessment for Indian sea states. Ocean Eng. 237, 109591.
- Chen, M., Xiao, P., Zhang, Z., Sun, L., Li, F., 2021. Effects of the end-stop mechanism on the nonlinear dynamics and power generation of a point absorber in regular waves. Ocean Eng. 242, 110123.
- Cheng, Z., Yang, J., Hu, Z., Xiao, L., 2014. Frequency/time domain modeling of a direct drive point absorber wave energy converter. Sci. China Phys. Mech. Astron. 57, 311–320.
- Chozas, J., Kofoed, J., Helstrup, N., 2014. The COE calculation tool for wave energy converters (Version 1.6, April 2014).
- Coe, R.G., Neary, V.S., 2014. Review of methods for modeling wave energy converter survival in extreme sea states.

- Crespo, A.J., Domínguez, J.M., Rogers, B.D., Gómez-Gesteira, M., Longshaw, S., Canelas, R., Vacondio, R., Barreiro, A., García-Feal, O., 2015. DualSPHysics: Opensource parallel CFD solver based on smoothed particle hydrodynamics (SPH). Comput. Phys. Comm. 187, 204–216.
- Cummins, W., Iiuhl, W., Uinm, A., 1962. The Impulse Response Function and Ship Motions. Citeseer.
- Da Silva, L.S., Cazzolato, B.S., Sergiienko, N.Y., Ding, B., Morishita, H.M., Pesce, C.P., 2020. Statistical linearization of the Morison's equation applied to wave energy converters. J. Ocean. Eng. Mar. Energy 6, 157–169.
- Davidson, J., Costello, R., 2020. Efficient nonlinear hydrodynamic models for wave energy converter design—A scoping study. J. Mar. Sci. Eng. 8 (1), 35.
- De Andres, A., Maillet, J., Todalshaug, J.H., Möller, P., Bould, D., Jeffrey, H., 2016. Techno-economic related metrics for a wave energy converters feasibility assessment. Sustain. (Switzerland) 8 (11).
- Dirlik, T., Benasciutti, D., 2021. Dirlik and tovo-benasciutti spectral methods in vibration fatigue: a review with a historical perspective. Metals 11 (9), 1333.
- Faedo, N., Olaya, S., Ringwood, J.V., 2017. Optimal control, MPC and MPC-like algorithms for wave energy systems: An overview. IFAC J. Syst. Control. 1, 37–56.
- Falnes, J., 2003. Ocean waves and Oscillating systems. In: Ocean Engineering, vol. 30, (7), p. 953.
- Fenton, J.D., Rienecker, M.M., 1982. A Fourier method for solving nonlinear water-wave problems: application to solitary-wave interactions. J. Fluid Mech. 118, 411-443.
- Folley, M., 2016. Numerical Modelling of Wave Energy Converters: State-Of-The-Art Techniques for Single Devices and Arrays. Academic Press.
- Folley, M., Babarit, A., Child, B., Forehand, D., Boyle, L.O., Silverthorne, K., Spinneken, J., Stratigaki, V., Troch, P., Folley, M., Babarit, A., Child, B., Forehand, D., Boyle, L.O., Child, B., 2019. A review of numerical modelling of wave energy converter arrays to cite this version: HAL Id: hal-01202077 a review of numerical modelling of wave energy converter arrays.
- Folley, M., Whittaker, T., 2010. Spectral modelling of wave energy converters. Coast. Eng. 57 (10), 892–897.
- Folley, M., Whittaker, T., 2013. Validating a spectral-domain model of an OWC using physical model data. Int. J. Mar. Energy 2, 1–11.
- Gao, Z., Merino, D., Han, K.-J., Li, H., Fiskvik, S., 2023. Time-domain floater stress analysis for a floating wind turbine. J. Ocean. Eng. Sci. 8 (4), 435–445.
- Gomez-Gesteira, M., Rogers, B.D., Dalrymple, R.A., Crespo, A.J., 2010. State-of-the-art of classical SPH for free-surface flows. J. Hydraul. Res. 48 (sup1), 6–27.
- González-Cao, J., Domínguez, J., Martínez-Estévez, I., Crespo, A., Gómez-Gesteira, M., Wang, S., Soares, C.G., 2024. Accuracy of the SPH-based solver DualSPHysics to reproduce hydrodynamic forces on bodies in a steady flow. In: Advances in Maritime Technology and Engineering. CRC Press, pp. 113–120.
- Guo, B., Ringwood, J.V., 2021. A review of wave energy technology from a research and commercial perspective. IET Renew. Power Gener. 15 (14), 3065–3090.
- Hals, J., Bjarte-Larsson, T., Falnes, J., 2002. Optimum reactive control and control by latching of a wave-absorbing semisubmerged heaving sphere. In: 21st International Conference on Offshore Mechanics and Arctic Engineering. pp. 415–423.
- IMARC Group, 2024. Stainless steel pricing report. (Accessed: 2024-12-19).
- Jimenez-Martinez, M., 2020. Fatigue of offshore structures: A review of statistical fatigue damage assessment for stochastic loadings. Int. J. Fatigue 132, 105327.
- Jin, S., Greaves, D., 2021. Wave energy in the UK: Status review and future perspectives. Renew. Sustain. Energy Rev. 143, 110932.
- Jin, S., Wang, D., Hann, M., Collins, K., Conley, D., Greaves, D., 2023. A designed two-body hinged raft wave energy converter: From experimental study to annual power prediction for the EMEC site using WEC-Sim. Ocean Eng. 267, 113286.
- Journée, J.M.J., Massie, W.W., Huijsmans, R.H.M., 2015. Offshore hydrodynamics. Kashiwagi, M., 2000. Non-linear simulations of wave-induced motions of a floating
- body by means of the mixed Eulerian-Lagrangian method. Proc. Inst. Mech. Eng. Part C: J. Mech. Eng. Sci. 214 (6), 841–855.
- Kebir, T., Correia, J., Benguediab, M., Jesus, A.M.d., 2021. Numerical study of fatigue damage under random loading using rainflow cycle counting. Int. J. Struct. Integr. 12 (1), 149–162.
- Kramer, M.M., Marquis, L., Frigaard, P., 2011. Performance evaluation of the wavestar prototype. In: Proceedings of the 9th European Wave and Tidal Conference. pp. 5–9.
- Kvittem, M.I., Moan, T., 2015. Time domain analysis procedures for fatigue assessment of a semi-submersible wind turbine. Mar. Struct. 40, 38–59.
- Lavidas, G., Venugopal, V., 2017. A 35 year high-resolution wave atlas for nearshore energy production and economics at the Aegean Sea. Renew. Energy 103, 401–417.
- Lawson, M., Yu, Y.-H., Ruehl, K., Michelen, C., et al., 2014. Development and demonstration of the WEC-sim wave energy converter simulation tool.
- Li, C., Dai, W., Duan, F., Zhang, Y., He, D., 2017. Fatigue life estimation of medium-carbon steel with different surface roughness. Appl. Sci. 7 (4), 338.
- Li, Y., Yu, Y.H., 2012a. A synthesis of numerical methods for modeling wave energy converter-point absorbers. Renew. Sustain. Energy Rev. 16 (6), 4352–4364.
- Liu, H., Wang, W., Tang, S., Mao, L., Mi, H., Zhang, G., Liu, J., 2019. Reliability assessment of water hydraulic-drive wave-energy converters. Energies 12 (21), 4189.
- Martinez, A., Iglesias, G., 2022. Mapping of the levelised cost of energy for floating offshore wind in the European Atlantic. Renew. Sustain. Energy Rev. 154, 111889.

- Martinez-Puente, E., Zarketa-Astigarraga, A., Esnaola, J., Zabala, A., Martinez-Astigarraga, M., Llavori, I., Penalba, M., 2023. On the modelling of fatigue assessment and lifetime estimation in marine energies. In: Proceedings of the 15th European Wave and Tidal Conference. Bilbao, Spain. p. 490.
- Merigaud, A., Gilloteaux, J.-C., Ringwood, J.V., 2012. A nonlinear extension for linear boundary element methods in wave energy device modelling. In: International Conference on Offshore Mechanics and Arctic Engineering, vol. 44915, American Society of Mechanical Engineers, pp. 615–621.
- Muñiz-Calvente, M., Álvarez-Vázquez, A., Pelayo, F., Aenlle, M., García-Fernández, N., Lamela-Rey, M., 2022. A comparative review of time-and frequency-domain methods for fatigue damage assessment. Int. J. Fatigue 163, 107069.
- Nielsen, K.M., Pedersen, T.S., Andersen, P., Ambühl, S., 2017. Optimizing control of wave energy converter with losses and fatigue in power take off. IFAC-PapersOnLine 50 (1), 14680–14685.
- Ogden, D., Ruehl, K., Yu, Y.-H., Keester, A., Forbush, D., Leon, J., Tom, N., 2022. Review of WEC-sim development and applications. Int. Mar. Energy J. 5 (NREL/JA-5700-83366).
- Palm, J., Eskilsson, C., 2021. On end-stops and snap loads for taut moored wave energy converters. In: Proc. 14th European Wave and Tidal Energy Conference. Plymouth, UK.
- Papillon, L., Costello, R., Ringwood, J.V., 2020. Boundary element and integral methods in potential flow theory: A review with a focus on wave energy applications. J. Ocean. Eng. Mar. Energy 6 (3), 303–337.
- Pastor, J., Liu, Y., 2014. Frequency and time domain modeling and power output for a heaving point absorber wave energy converter. Int. J. Energy Environ. Eng. 5 (2–3). 1–13.
- Pecher, A., 2017. Handbook of Ocean Wave Energy, vol. 7.
- Penalba, M., Kelly, T., Ringwood, J., 2017a. Using NEMOH for modelling wave energy converters: A comparative study with WAMIT. In: 12th European Wave and Tidal Energy Conference. p. 10.
- Penalba, M., Kelly, T., Ringwood, J., 2017b. Using NEMOH for modelling wave energy converters: A comparative study with WAMIT.
- Penalba Retes, M., Giorgi, G., Ringwood, J., 2015. A review of non-linear approaches for wave energy converter modelling. In: Proceedings of the 11th European Wave and Tidal Energy Conference. European Wave and Tidal Energy Conference 2015.
- Petracca, E., Faraggiana, E., Ghigo, A., Sirigu, M., Bracco, G., Mattiazzo, G., 2022.

 Design and techno-economic analysis of a novel hybrid offshore wind and wave energy system. Energies 15 (8), 2739.
- Polinder, H., 2013. Principles of electrical design of permanent magnet generators for direct drive renewable energy systems. In: Electrical Drives for Direct Drive Renewable Energy Systems. Woodhead Publishing Limited, pp. 30–50.
- Prado, M., Polinder, H., 2013. Direct drive wave energy conversion systems: An introduction. Electrical Drives for Direct Drive Renewable Energy Systems. Woodhead Publishing Limited, pp. 175–194.
- Quigley, J.P., Lee, Y.-L., Wang, L., 2016. Review and assessment of frequency-based fatigue damage models. SAE Int. J. Mater. Manuf. 9 (3), 565–577.
- Raghavan, V., Lavidas, G., Metrikine, A., 2024. Comparing open-source BEM solvers for analysing wave energy converters. 2647, (7), IOP Publishing, 072002,
- Ransley, E., Greaves, D., Raby, A., Simmonds, D., Hann, M., 2017. Survivability of wave energy converters using CFD. Renew. Energy 109, 235–247.
- Ricci, P., António, A.F., Saulnier, J.B., Pontes, M.T., 2008. Time-domain models and wave energy converters performance assessment. In: Proceedings of the International Conference on Offshore Mechanics and Arctic Engineering - OMAE, vol. 6, pp. 699–708.
- van Rij, J., Yu, Y.-H., Guo, Y., Coe, R.G., 2019. A wave energy converter design load case study. J. Mar. Sci. Eng. 7 (8), 250.
- Roberts, J.B., Spanos, P.D., 2003. Random Vibration and Statistical Linearization. Courier Corporation.
- Rosati, M., Ringwood, J.V., 2023. Control co-design of power take-off and bypass valve for OWC-based wave energy conversion systems. Renew. Energy 219, 119523.
- Ruehl, K., Michelen, C., Bosma, B., Yu, Y.-H., 2016. WEC-sim phase 1 validation testing: Numerical modeling of experiments. In: International Conference on Offshore Mechanics and Arctic Engineering, vol. 49972, American Society of Mechanical Engineers, V006T09A026.
- Ruehl, K., Michelen, C., Kanner, S., Lawson, M., Yu, Y.-H., 2014. Preliminary verification and validation of WEC-sim, an open-source wave energy converter design tool. In: International Conference on Offshore Mechanics and Arctic Engineering, vol. 45547, American Society of Mechanical Engineers, V09BT09A040.

- Rusu, E., Onea, F., 2018. A review of the technologies for wave energy extraction.

 Clean Energy 2 (1), 10–19.
- Shahroozi, Z., Göteman, M., Engström, J., 2022. Fatigue analysis of a point-absorber wave energy converter based on augmented data from a WEC-sim model calibrated with experimental data. Trends Renew. Energies Offshore 925–933.
- Sheng, W., Tapoglou, E., Ma, X., Taylor, C.J., Dorrell, R.M., Parsons, D.R., Aggidis, G., 2022. Hydrodynamic studies of floating structures: Comparison of wave-structure interaction modelling. Ocean Eng. 249, 110878.
- Shipbuilding Steel, 2024. Price for AH36 steel plate for shipbuilding. (Accessed: 2024-12-19).
- Silva, L.S.P.d., 2019. Nonlinear Stochastic Analysis of Wave Energy Converters Via Statistical Linearization (Master thesis). Universidade de São Paulo.
- Silva, L., Sergiienko, N., Pesce, C., Ding, B., Cazzolato, B., Morishita, H., 2020. Stochastic analysis of nonlinear wave energy converters via statistical linearization. Appl. Ocean Res. 95, 102023.
- Taghipour, R., Moan, T., 2008. Efficient frequency-domain analysis of dynamic response for the multi-body wave energy converter in multi-directional wave. In: ISOPE International Ocean and Polar Engineering Conference. ISOPE, pp. ISOPE–I.
- Tan, J., Jarquin Laguna, A., Polinder, H., Miedema, S., 2022a. The application of the spectral domain modeling to the techno-economic analysis of the adjustable draft point absorbers. In: International Conference on Offshore Mechanics and Arctic Engineering, vol. 85932, American Society of Mechanical Engineers, V008T09A067.
- Tan, J., Laguna, A.J., 2023. Spectral-domain modelling of wave energy converters as an efficient tool for adjustment of PTO model parameters. In: Proceedings of the European Wave and Tidal Energy Conference, vol. 15.
- Tan, J., Polinder, H., Laguna, A.J., Miedema, S., 2022b. The application of the spectral domain modeling to the power take-off sizing of heaving wave energy converters. Appl. Ocean Res. 122, 103110.
- Tan, J., Polinder, H., Laguna, A.J., Wellens, P., Miedema, S.A., 2021. The influence of sizing of wave energy converters on the techno-economic performance. J. Mar. Sci. Eng. 9 (1), 52.
- Tan, J., Polinder, H., Wellens, P., Miedema, S., 2020. A feasibility study on downsizing of power take off system of wave energy converters. In: Developments in Renewable Energies Offshore. CRC Press, pp. 140–148.
- Tan, J., Tao, W., Laguna, A.J., Polinder, H., Xing, Y., Miedema, S., 2023. A spectral-domain wave-to-wire model of wave energy converters. Appl. Ocean Res. 138, 103650
- Tan, J., Wang, X., Polinder, H., Laguna, A.J., Miedema, S.A., 2022c. Downsizing the linear PM generator in wave energy conversion for improved economic feasibility. J. Mar. Sci. Eng. 10 (9), 1316.
- Teng, B., Taylor, R.E., 1995. New higher-order boundary element methods for wave diffraction/radiation. Appl. Ocean Res. 17 (2), 71–77.
- Tom, N., Lawson, M., Yu, Y.-H., 2015. Recent additions in the modeling capabilities of an open-source wave energy converter design tool. In: ISOPE International Ocean and Polar Engineering Conference. ISOPE, ISOPE-I.
- Wei, Y., Yu, Z., Berglind, J.d.B., van Rooij, M., Prins, W., Jayawardhana, B., Vakis, A.I., 2017. A frequency-domain model for a novel wave energy converter. In: European Wave and Tidal Energy Conference Series. EWTEC.
- Zhong, W., Yu, H., Wang, H., Zhang, J., 2024. Lowering the levelized cost of energy (LCOE) for mass-adjustable-buoy-based wave energy converters. Ocean Eng. 311, 118878.
- Zurkinden, A.S., Lambertsen, S.H., Damkilde, L., Gao, Z., Moan, T., 2013. Fatigue analysis of a wave energy converter taking into account different control strategies.
 In: International Conference on Offshore Mechanics and Arctic Engineering, vol. 55423, American Society of Mechanical Engineers, V008T09A057.
- Zurkinden, A.S., Lambertsen, S.H., Damkilde, L., Gao, Z., Moan, T., 2015. Fatigue analysis of a point absorber wave energy converter subjected to passive and reactive control. J. Offshore Mech. Arct. Eng. 137 (5), 051901.